

**XPS AND CORROSION STUDIES
ON ZINC PHOSPHATE TREATED SURFACES OF ALUMINUM**

by

WAI FAN HEUNG

B.Sc., University of British Columbia, 1991

**A THESIS SUBMITTED IN PARTIAL FULFILLMENT OF
THE REQUIREMENTS FOR THE DEGREE OF
MASTER OF SCIENCE**

in

**THE FACULTY OF GRADUATE STUDIES
DEPARTMENT OF CHEMISTRY**

**We accept this as conforming
to the required standard**

THE UNIVERSITY OF BRITISH COLUMBIA

October 1993

© Wai Fan Heung, 1993

In presenting this thesis in partial fulfilment of the requirements for an advanced degree at the University of British Columbia, I agree that the Library shall make it freely available for reference and study. I further agree that permission for extensive copying of this thesis for scholarly purposes may be granted by the head of my department or by his or her representatives. It is understood that copying or publication of this thesis for financial gain shall not be allowed without my written permission.

Department of CHEMISTRY

The University of British Columbia
Vancouver, Canada

Date Nov 12, 1993

Abstract

The work in this thesis deals with an investigation of zinc phosphate (ZPO) treated surfaces of 7075-T6 aluminum alloy. X-ray photoelectron spectroscopy (XPS) and corrosion tests are used to characterize the treated surfaces and to examine their corrosion protection performance.

The coating processes are performed by immersing polished alloy surfaces into 10 wt. % of ZPO suspension in water adjusted at various pH conditions. Biased XPS is applied to discriminate the physically trapped and chemically absorbed zinc compounds in the ZPO treated surfaces. Ultrasonic rinsing in distilled water for the treated surfaces is found important in the sample preparation procedure so as to remove any physically trapped compounds from the surfaces.

Five different pH conditions (pH=3.5, 5.0, 6.6, 10.5, and 13.0) are studied in this work. Acetic acid and sodium hydroxide solution are used to adjust the required pHs for the ZPO solutions. The treated surfaces are studied by angle dependent XPS (ADXPS) to obtain chemical information at different probed depths. ZPO is found to be an effective coating compound for the 7075-T6 aluminum surface. At pH=6.6 and 3.5, the coatings found on the treated surfaces are believed to be respectively a ZnO_x-AlO_x mixed material and a thin ZPO-like compound. In alkaline and weakly acidic conditions (pH=13.0, 10.5 and 5.0), the coatings formed on the surfaces are enhanced and have structures with mixed ZnO_x-AlO_x-ZPO materials.

Weight loss measurements, atomic absorption spectrometry (AAS) and scanning electron microscopy (SEM) are involved in the corrosion studies. 3.5 % NaCl solutions are used as the corrosive environments. Surfaces before and after the corrosion tests are

compared to examine the corrosion protection performance of each surface. As judged by XPS, the surface prepared at pH=13.0 is likely to provide the best corrosion control among the five treated surfaces. Dissolution of aluminum from the alloy is observed in the corrosive environment. The coating is believed to play a role as a physical barrier to suppress the corrosion attack on aluminum.

Table of Contents

Abstract.....	ii
Table of Contents	iv
List of Tables.....	vii
List of Figures	viii
Acknowledgments	xi
Chapter 1 Introduction.....	1
1.1 General	1
1.2 Chemical Conversion Coating.....	4
1.3 Surface Analytical Techniques Applied to Coating and Corrosion Studies	5
1.4 Aims of this Research.....	7
Chapter 2 Experimental Methods.....	10
2.1 X-ray Photoelectron Spectroscopy	11
2.1.1 Introduction.....	11
2.1.2 Basic Concepts	12
(A) Principles	12
(B) Surface Sensitivity of XPS.....	21
2.1.3 Chemical Analyses with XPS.....	23
(A) Qualitative Analysis.....	23
(B) Quantitative Analysis.....	28
2.1.4 Angle Dependent XPS	30
2.1.5 Bias Technique Applied on XPS.....	33

2.1.6	Instrumentation of XPS.....	35
(A)	Ultra-High Vacuum.....	35
(B)	Excitation Source.....	38
(C)	Sample Handling.....	41
(D)	Electron Energy Analyzer.....	41
(E)	Detector.....	46
2.2	Scanning Electron Microscopy.....	48
2.2.1	Background.....	48
2.2.2	System Used.....	48
2.3	Weight Loss Measurements.....	52
2.4	Atomic Absorption Spectrometry.....	53
Chapter 3	Coating and Corrosion Studies on ZPO treated Aluminum Surfaces.....	54
3.1	Coating Studies on Zinc Phosphate Treated Aluminum Surfaces.....	54
3.1.1	Sample Preparations.....	54
3.1.2	XPS Measurements.....	54
3.1.3	Results and Discussion.....	57
(A)	The Aluminum Control Panel (Sample A).....	57
(B)	The Aluminum Panel Treated in Natural ZPO Solution at pH=6.6 (Samples B and C).....	60
(C)	The Aluminum Panel Treated in ZPO Solution at Various pH Values (Samples D to G).....	66
(1)	Strongly Alkaline Coating Solution (pH=13.0; Sample D).....	72
(2)	Moderately Alkaline Coating Solution (pH=10.5; Sample E).....	73

(3) Moderately Acidic Coating Solution (pH=5.0; sample F).....	73
(4) Strongly Acidic Coating Solution (pH=3.5; sample G).....	75
3.2 Corrosion Studies on Zinc Phosphate Treated Aluminum Surfaces.....	76
3.2.1 Sample Preparations.....	76
3.2.2 Results and Discussion.....	80
(A)Part I: Initial Studies.....	80
(B)Part II: Further Studies.....	86
Chapter 4 Concluding Remarks and Future Work	90
4.1 Concluding Remarks	90
4.2 Future Work.....	91
References.....	93

List of Tables

Table 1.1	Features of various surface analytical methods.	8
Table 2.1	A table of some characteristic X-ray lines.....	17
Table 2.2	A summary of the atomic orbital nomenclature.	25
Table 2.3	The Auger parameters for zinc compounds.	29
Table 3.1	Sample descriptions.	55
Table 3.2	Elemental composition and atomic ratios for blank Al surface (sample A) with varying take-off angle.....	59
Table 3.3	Elemental composition and atomic ratios for ZPO treated Al surface (sample C) with varying take-off angle.....	64
Table 3.4	A list of binding energies (in eV) of zinc, phosphorus on ZPO treated aluminum surfaces and the ZPO reference compound.	68
Table 3.5	Atomic ratios for samples C, D, E, F, G, and the ZPO reference compound with varying take-off angle.	71
Table 3.6	Zn/Al ratios for samples A, A1, C and C1 with varying take-off angle.....	81
Table 3.7	Qualitative observations from XPS for samples after immersion in NaCl solution.	87

List of Figures

Figure 1.1	The natural oxide layer formed on an aluminum surface.	2
Figure 1.2	Difference between metallic and oxide type protective layers on aluminum.....	2
Figure 1.3	Comparison between bulk and surface analysis.....	6
Figure 2.1	A schematic diagram of the photoemission process.	13
Figure 2.2	The experimental setting for XPS.	14
Figure 2.3	(a) An illustration of X-rays produced from electronic transitions. (b) Approximated energy distribution of unmonochromatized Al radiation, showing the strong characteristic $K\alpha$ and $K\beta$ lines and the Bremsstrahlung radiation.....	16
Figure 2.4	Reference levels for a metal sample and a spectrometer.....	18
Figure 2.5	A schematic diagram of the Auger process.....	20
Figure 2.6	The compilation by Seah and Dench of measurements of the inelastic mean free path, λ , for different elements.	22
Figure 2.7	XPS survey scan spectrum of copper, with an insert of the Cu LMM Auger series.	24
Figure 2.8	Spin-orbit splitting for the Zn 2p photoelectron peaks.	25
Figure 2.9	High resolution XPS spectrum of the Al 2p photoelectron peak from an aluminum alloy with naturally formed oxide layer.	27
Figure 2.10	Illustration of the principle of angle dependent XPS (ADXPS).....	31
Figure 2.11	Theoretical angular dependent curves for a flat clean surface coated with an overlayer.	31
Figure 2.12	Zn $2p_{3/2}$ photoelectron peaks from a zinc phosphate treated aluminum sample. Curve 1 is obtained from the grounded sample.	

	Curve 2 is obtained from the sample with -94 V biased potential applied on the sample and shifted back by 94 eV after measuring	34
Figure 2.13	A schematic indication of the Leybold MAX 200 spectrometer (a) top view (b) side view.....	36
Figure 2.14	Components of the MAX 200 analysis chamber.	37
Figure 2.15	The pumping system of the XPS spectrometer.	39
Figure 2.16	A schematic diagram of the Al and Mg dual anode X-ray source.....	40
Figure 2.17	The MAX 200 system: sample handling assembly.	42
Figure 2.18	The analysis and transfer chambers of the spectrometer in MAX 200 system.	43
Figure 2.19	A schematic diagram of a concentric hemispherical analyzer (CHA).	44
Figure 2.20	(a) A cutaway view of a microchannel plate, (b) a schematic diagram of a microchannel plate assembly.	47
Figure 2.21	A schematic diagram of a scanning electron microscope (SEM).	49
Figure 2.22	The illuminating / imaging system of a SEM unit.....	50
Figure 3.1	A flow chart summarizing the sample preparation procedure for the coating process.....	56
Figure 3.2	XPS survey spectrum for sample A, a blank Al surface.	58
Figure 3.3	XPS survey spectrum for sample C, ZPO treated Al surface prepared at natural pH.	61
Figure 3.4	High resolution Zn 2p _{3/2} spectra for: (a) sample C, $\theta = 90^\circ$; (b) sample C, $\theta = 30^\circ$; (c) sample B, $\theta = 90^\circ$; (d) sample B, $\theta = 30^\circ$; (e) sample B, $\theta = 90^\circ$ after bias potential; (f) sample B, $\theta = 30^\circ$ after bias potential.	62
Figure 3.5	Proposed surface morphologies for (a) sample B, (b) sample C, (c) samples D & E, (d) sample F and (e) sample G.	65

Figure 3.6	XPS survey spectrum for sample D, ZPO treated Al surface prepared at pH=13.0.....	67
Figure 3.7	pH effect on the atomic ratios of elements on the ZPO treated Al surfaces (a) before and (b) after corrosion tests (values obtained at take-off angle equal 90°).....	70
Figure 3.8	Sample preparation steps for Part I (initial studies) of corrosion studies.....	77
Figure 3.9	Sample preparation steps for Part II (further studies) of corrosion studies.....	79
Figure 3.10	SEM micrographs of : (a) sample A, blank aluminum; (b) sample A1, sample A after corrosion; (c) sample C, ZPO treated aluminum; (d) sample C1, sample C after corrosion.	83
Figure 3.11	Photographs taken from surfaces after the 5 hours corrosion tests, (a) sample A, blank Al; (b) sample A2, sample A after corrosion; (c) sample D, ZPO treated surface prepared at pH=13.0; (d) sample D2, sample D after corrosion.	89

Acknowledgments

I would like to thank my supervisor, Professor K.A.R. Mitchell, for his sponsoring this work and his helpful comments and advice on this thesis. I am especially grateful to Dr. P.C. Wong, Professor Y.P. Yang and Professor M.Y. Zhou for their active involvement, and helpful discussions in this work. I also thank Dr. Y.S. Li for teaching me the sample polishing procedure. I also acknowledge the staff from the electrical workshop for maintaining the instruments in working order and the staff from the mechanical workshop for preparing the necessities for this research. I also appreciate the help from the microscope laboratory in the Department of Metals and Materials Engineering for the SEM investigation. I also acknowledge the financial support provided by the Defence Research Establishment Pacific (DREP) and thank Dr. Terry Foster for his comments on this work.

In addition, I am very grateful to my group members, Y.L. Leung, Y.M. Wang, W. Liu, K.C. Wong, D-T Vu Grimsby, Bernie Flinn and Harman Cheng for their "always available" help in the laboratory, and my friends for their prayers and encouragement in these two years. Finally, I would like to thank my parents and my brother for their support and encouragement.

Chapter 1 Introduction

1.1 General

Metals have played an important role in the development of civilization, and in recent times aluminum, copper, zinc, iron and steel have been very widely used. Among these, aluminum has a vital role in the light metal industry. Its applications in everyday life include household usage as well as uses in mechanical apparatus, the chemical and food industry, architecture, transportation and so forth [1.1].

The main properties on which the applications of aluminum are based are its low density of approximately 2.7 g/cm^3 [1.2], its high mechanical strength achieved by alloying and heat treatments, and the relatively high corrosion resistance of the metal. The chief alloying constituents added to aluminum are copper, magnesium, silicon, manganese, nickel and zinc. Generally, the higher the purity of aluminum, and its alloys, the greater the corrosion resistance [1.3]. The excellent corrosion resistance of aluminum is due to its affinity for oxygen; a very thin oxide film covers the surface as soon as a freshly-cut piece of the metal is exposed to the atmosphere [1.4].

In general, this air-formed film is believed to be porous and amorphous, with the outer surface being a hydrated aluminum oxide (Figure 1.1). Its thickness ranges from 1 to 3 nm. This firmly adhered oxide film is insoluble in water, and many other chemicals, and helps protect the underlying metal from foreign attack. Breakdown of the oxide film can result from mechanical rupture, or from chemical attack by anions

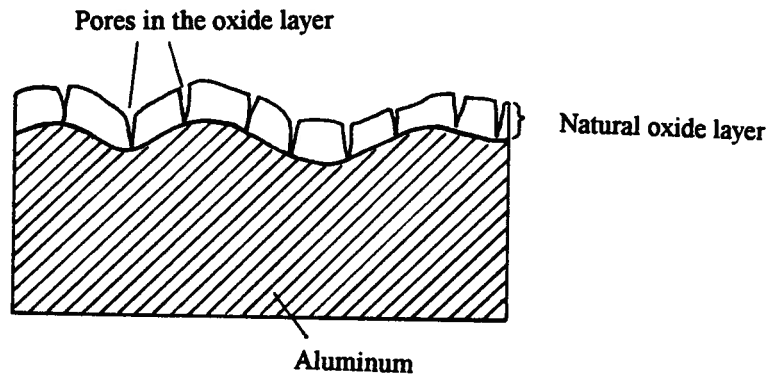


Figure 1.1 The natural oxide layer formed on an aluminum surface.

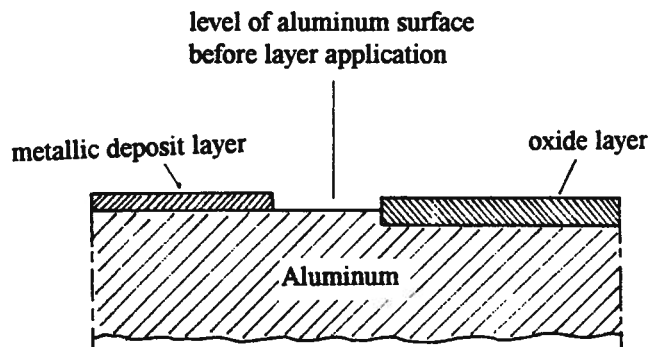
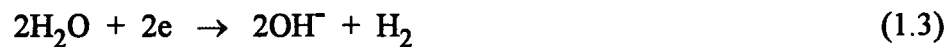


Figure 1.2 Difference between metallic and oxide type protective layers on aluminum.

such as chloride ions. A consequence of the film breakdown is corrosion [1.5]. Corrosion is generally defined as a gradual wearing away of metal by a chemical or electrochemical oxidizing process [1.6]. In normal situations, repair of the oxide film is immediate and can be accompanied by the oxygen reduction reaction or the hydrogen evolution reaction as shown here:



} (Cathodic reaction)



Therefore, aluminum oxide or aluminum hydroxide can be formed. However, in the presence of aggressive ions, this repassivation process is hindered, and soluble complex ions, e.g. $\text{Al}(\text{OH})_2\text{Cl}_2^-$, may be formed [1.7] with consequent dissolution and thinning of the metal component.

A obvious way to prevent the aluminum corrosion is to avoid oxidizing or aggressive species coming in contact with the metal surface, on which the corrosion is always initiated. This may be done by applying a coating layer to the surface. The protection capacity of a coating (i.e. its service life), depends both on its physical thickness and on its chemical durability in a particular environment. The types of coating layers applied on metal surfaces can be divided into two main categories: metallic coatings and oxide coatings, as shown in Figure 1.2 [1.8]. In the first type, a metal or metal alloy will be sprayed, cladded or deposited on to the aluminum surface for corrosion protection. However, this layer sometimes suffers problems of mechanical strength and elongation,

and results in cracking. The oxide-type coating layer is usually used as a base for organic finishes. Chemical methods (e.g. chemical conversion treatments), or electrolytic methods (e.g. anodizing), are applied to the metal to produce oxide-type coating layers whose thicknesses may vary from 2 to 100 nm, and the compositions may show different oxides and other compounds, depending on the reaction conditions. In this thesis, chemical conversion treatments will be emphasized.

1.2 Chemical Conversion Coating

In forming a chemical conversion coating, the metal surface is immersed into a coating solution, from which the coating compounds react and incorporate with the metal surface. Although an oxide conversion coating can be used without further treatment, its function is normally to act as an undercoat and a base for organic finishes [1.9, 1.10], in order to improve the adhesion of paints and adhesives.

The main attraction of finishes obtained by chemical conversion is the economy and the speed with which they can be produced. Compared with anodizing treatments, chemical conversion treatments require a plant with simple construction and relatively low consumption of electric power; also coatings can be produced rapidly on a large number of articles. All these factors make for an economic process [1.9].

Zinc chromate is one of the most extensively used and efficient coating compounds for aluminum [1.10, 1.11]. This chromate coating forms a continuous layer which acts as a barrier to reduce the active surface area on base metal, and delay the transportation of oxidizing and aggressive species. However, chromates have been found to cause irritation of the respiratory tract, and produce lung cancer in workers employed in chromium

manufacturing plants [1.12, 1.13]. Because of these toxicological concerns, new chromate-free coatings are being evaluated for effective corrosion control [1.12, 1.14-1.15]. Among several non-toxic and anti-corrosive coatings so far developed, users and manufacturers have mainly focused their attention on zinc phosphate.

Zinc phosphate is an established coating treatment for steel [1.16-1.19]. The coating on steel, resulting from the formation of a mixed iron phosphate and zinc iron phosphate coating layer, functions as an intermediate layer to improve the adhesion of paint, thereby increasing the corrosion resistance of the painted products [1.20, 1.21]. The phosphate coatings are used in highly corrosive applications such as car bodies, household appliances, structural steel and the like [1.22]. Because of its anti-corrosion property, zinc phosphate is being considered for application to aluminum as well.

1.3 Surface Analytical Techniques Applied to Coating and Corrosion Studies

Analytical investigations of a coating layer on a metal surface can give knowledge about the composition and structure of the layer, and possibly about the mechanism of the coating process. Studies of the corrosion protection performance of a treated surface provide an evaluation of the anti-corrosion ability of the coating layer. All this information helps to determine the best coating for a particular metal substrate. Both coating and corrosion processes on a metal are initiated at the outermost surface layers. Frequently, the chemical and physical properties of the surface region of a solid are different from those in the bulk [1.23]. As a result, surface sensitive techniques are required in order to provide the most detailed knowledge. Figure 1.3 [1.24] compares the bulk and the surface analytical approaches. By definition, surface analysis is concerned with the analysis of the

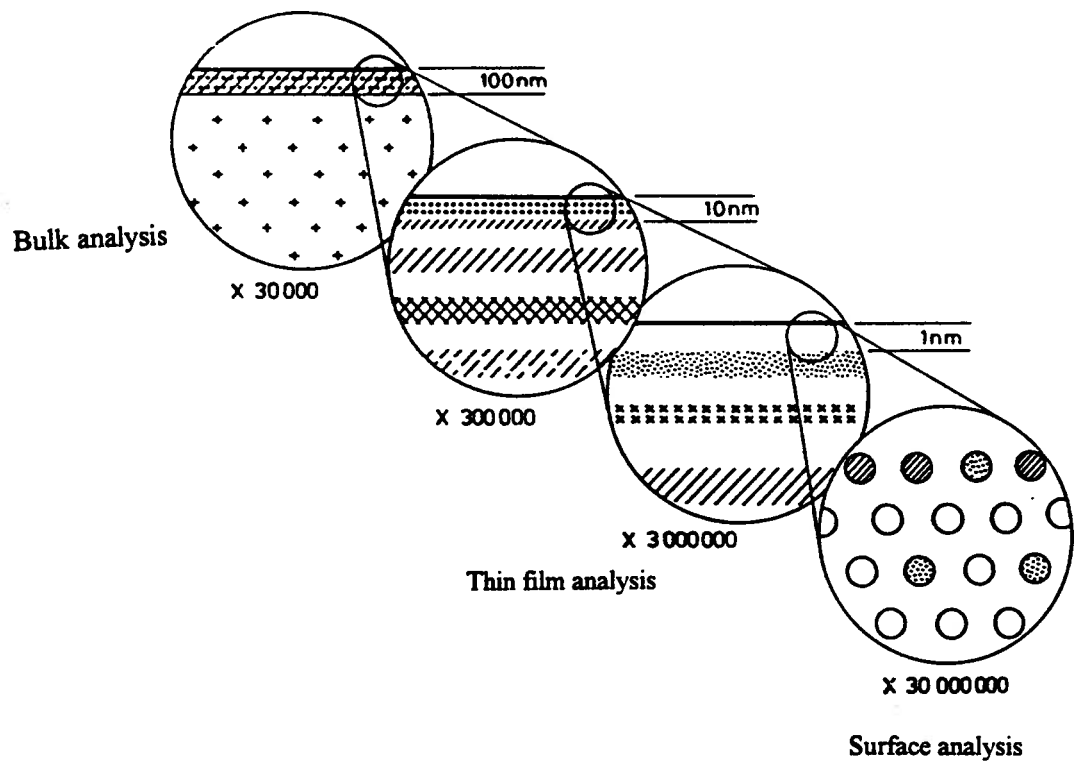


Figure 1.3 Comparison between bulk and surface analysis.

elemental composition, the chemical state, the surface structure and morphology of the outermost atomic layers of a solid. The most commonly used surface analytical methods include X-ray photoelectron spectroscopy (XPS), Auger electron spectroscopy (AES), and secondary ion mass spectroscopy (SIMS). Their major characteristics are listed on Table 1.1 and their sampling depths are especially in the 1 to 5 nm range.

1.4 Aims of this Research

The motivation for the work in this thesis originated from a contract with the Defence Research Establishment Pacific (DREP) to study various corrosion protection treatments on aluminum alloys. The present investigation concentrates on the coating and corrosion protection performance of zinc phosphate, as a possible replacement for zinc chromate, on 7075-T6 aluminum alloy, which has long been used in the aircraft and automobile industries because of its favourable strength-to-weight ratio and high durability [1.27].

The primary goal of the work is to determine whether zinc phosphate can be effectively coated (i.e. chemically absorbed) into the aluminum alloy. The treated surfaces are characterized by XPS, in order to investigate the compositions and morphologies of the coating layers, with a special emphasis on determining the amounts of zinc and phosphate present.

The next objective is to establish optimal conditions for coating maximum amounts of zinc and phosphorus by adjusting the acidities and basicities of the coating solutions. In addition, XPS is used in attempts to learn about the coating mechanisms of zinc phosphate

Table 1.1 Features of various surface analytical methods

Analytical methods	Brief description	Information	Ref.
X-ray photoelectron spectroscopy (XPS)	Core level photoelectrons emitted from surface atoms by X-ray excitation	Composition and chemical state	1.24
Auger electron spectroscopy (AES)	Study Auger electrons emitted from surface atoms after excitation by X rays or energetic electrons	Composition	1.24
Secondary ion mass spectroscopy (SIMS)	Mass analysis of sputtered ions resulting from bombardment by energetic primary ions	Composition	1.25

onto the aluminum alloy and the morphologies of the treated surfaces.

The third objective of the study is to evaluate the corrosion protection performance of these treated surfaces. No paints are applied on these treated surfaces, so that the corrosion protection ability of the zinc phosphate coating layer can be studied without other influencing factors. A 3.5% sodium chloride solution is used to perform immersion corrosion tests for these surfaces [1.28], over periods ranging from 2 to 5 hours. The surfaces are compared before and after the corrosion tests. In order to gain maximum information on the process, other analytical methods are employed for the evaluation, including scanning electron microscopy (SEM), weight loss measurements and atomic absorption spectrometry (AAS).

Chapter 2 Experimental Methods

Four main methods are used in this work. They are X-ray photoelectron spectroscopy (XPS), scanning electron microscopy (SEM), weight loss measurements and atomic absorption spectrometry (AAS). XPS is used to characterize the sample surfaces both after the coating processes and after the corrosion tests. Samples are prepared in an atmospheric environment and are introduced into the spectrometer for analysis. Details about the principles and instrumentation of XPS will be discussed in the following section. The evaluation of the corrosion protection performance of the treated surfaces is done by SEM, weight loss measurements and AAS. Scanning electron micrographs at 4000 magnification are taken from surfaces before and after corrosion tests. Weight loss measurements and AAS are employed to determine the corrosion rate of each sample and to detect the dissolution of aluminum in the corrosive environment. The details for these two methods will also be discussed in this chapter.

2.1 X-ray Photoelectron Spectroscopy

2.1.1 Introduction

X-ray photoelectron spectroscopy (XPS) is generally regarded as an important technique for surface characterization and analysis. This technique, also called ESCA (electron spectroscopy for chemical analysis), provides compositional analysis (except for hydrogen and helium), for the topmost layers of a solid surface. Chemical bonding state information can also be provided [2.1].

XPS has its origin in investigations of the photoelectric effect, which was discovered by Hertz in 1887 [2.2]. He produced photoelectrons by illuminating matter by ultraviolet light. Einstein, in 1905, established the relationship between the kinetic energy of a photoelectron, the binding energy in the solid, the radiation energy and the work function of a solid [2.3]. Before World War I, Moseley, Rawlison and Robinson carried out experiments in this new field. After the war, Robinson and Maurice de Broglie continued the work separately and gave rapid development for the subject. However, that work finished, without any major advance in resolution or sensitivity, at the outbreak of World War II.

Starting from the late 1940's, decisive developments were underway in Sweden. Siegbahn developed the technique of β -ray spectroscopy to high levels of precision and then realized that X-rays could also be used for the excitation. Improvements in resolving power were obtained by utilizing a double-focusing spectrometer. Later, Siegbahn's group successfully observed photoelectron peaks and thus was able to measure the electron binding energy more accurately. This group also observed the chemical shift effects in core-level binding energies, and continued to develop the whole field of electron

spectroscopy from 1955 to 1970. Commercial instruments started to appear in the mid 1960's. In 1972, Brundle and Roberts performed XPS studies on carefully prepared surfaces under ultra-high vacuum, and that work established XPS as a surface analytical technique [2.4].

2.1.2 Basic Concepts

(A) Principles

XPS depends on photoemission. The process is shown in Figure 2.1. If a photon of energy $h\nu$ entirely transfers its energy to an electron with binding energy E_b (where $h\nu > E_b$), for example in the core level of an atom, the kinetic energy (E_k) of an emitted photoelectron will be approximated by:

$$E_k \cong h\nu - E_b \quad (2.1)$$

Since different elements have different sets of electronic binding energies, measurements of the kinetic energies of photoelectrons from a sample can provide elemental identification.

An overview of the experimental setting for XPS is shown in Figure 2.2. X-rays with fixed energy $h\nu$ bombard onto a sample and result in the emission of photoelectrons. These photoelectrons are then directed into the electron analyzer for energy analysis and their intensities are measured by a detector. All these data are processed by a computer system and an XPS spectrum, usually plotted as intensity against binding energy, is

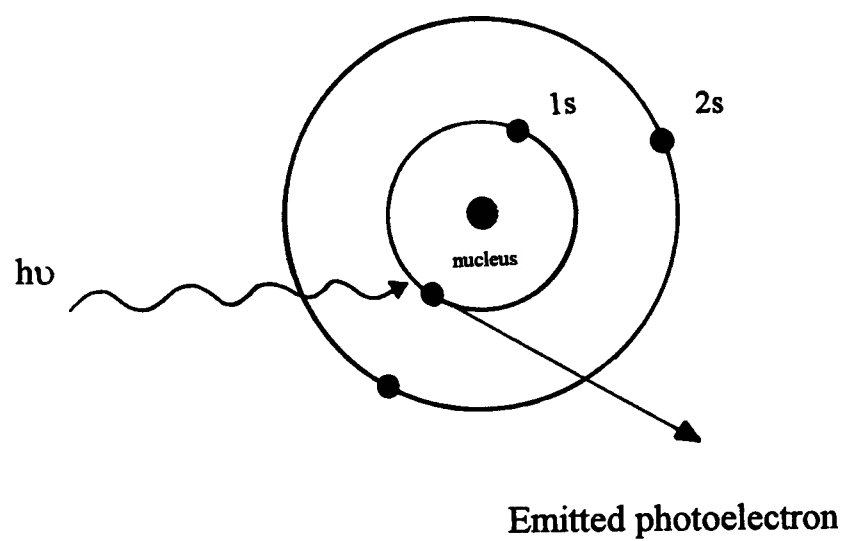


Figure 2.1 A schematic diagram of the photoemission process.

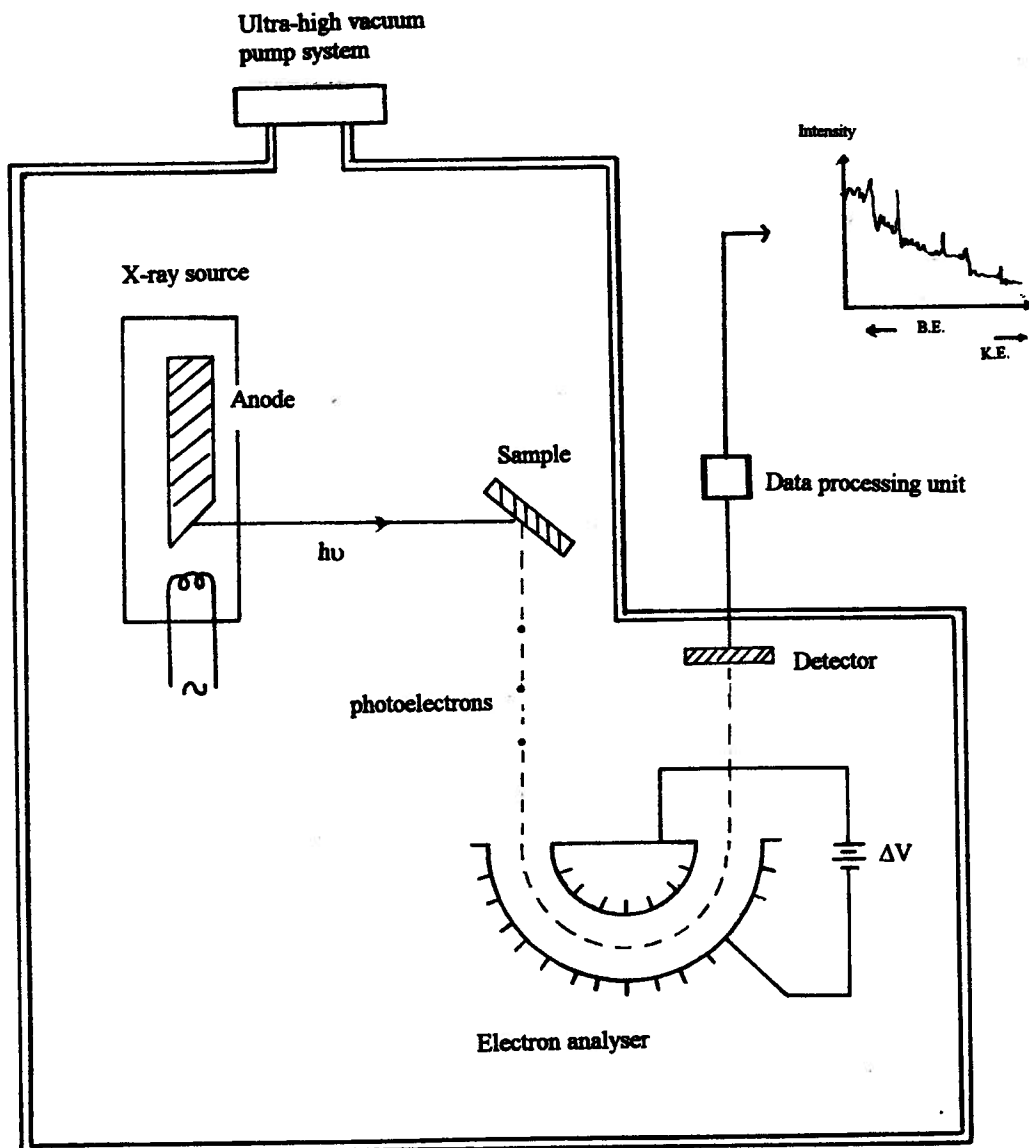


Figure 2.2 The experimental setting for XPS.

generated. As shown from the figure, XPS analysis is performed under a ultra-high vacuum system (section 2.1.6 (A)).

The X-rays used in XPS are characteristic emission lines generated from an anode bombarded by high energy electrons emitted from a heated filament. The energies of these characteristic lines are dependent on the electronic transitions within the anode atoms (Figure 2.3(a)) [2.5]. Besides these characteristic lines, a continuous spectrum, known as Bremsstrahlung radiation, is also produced (Figure 2.3(b) [2.6]). In choosing a suitable anode material for XPS, the line width of the characteristic emission line is in major consideration. The line width determines the energy resolution of a spectrum (section 2.1.6 (D)). Another consideration is that the anode material must be a good conductor, otherwise heat transfer from the point of impingement of the electrons to stimulate the X-rays will be insufficient and the anode might melt. Table 2.1 [2.7] lists the energies and the widths of some characteristic X-ray lines of some materials. The most commonly used X-ray lines in XPS are the $K\alpha$ lines of Al and Mg which have line widths of 0.85 eV and 0.70 eV and energies of 1486.6 eV and 1253.6 eV, respectively.

For a metallic solid, the binding energy (E_b) of an electron is referenced to the Fermi level, which is defined as the highest occupied energy level. The Fermi level is below the vacuum level by the work function (W_m), i.e. the energy which must be supplied for an electron to escape from the metal (Figure 2.4). Therefore, the kinetic energy (E_k) of an electron emitted from a metal surface is:

$$E_k = h\nu - E_b - W_m \quad (2.2)$$

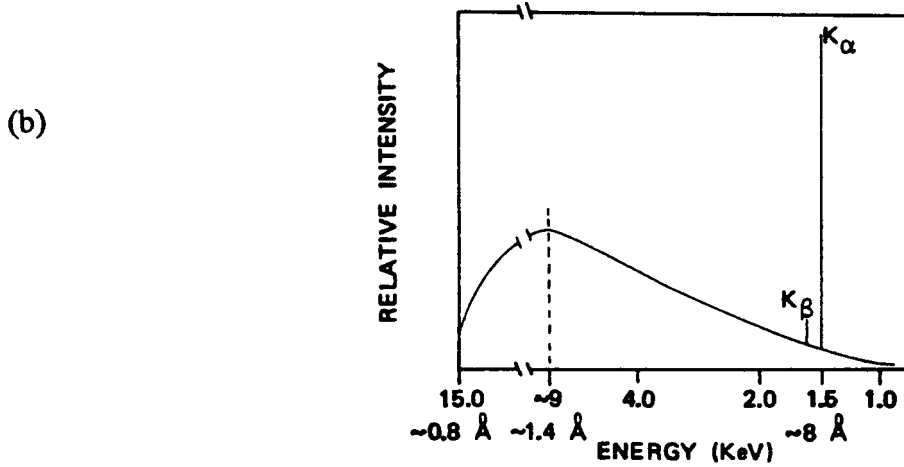
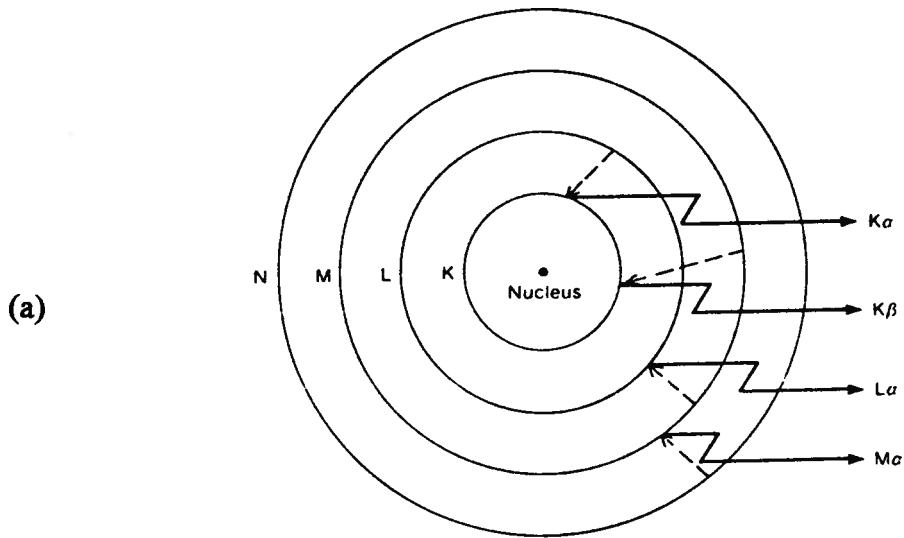


Figure 2.3 (a) An illustration of X-rays produced from electronic transitions. (b) Approximated energy distribution of unmonochromatized Al radiation, showing the strong characteristic $K\alpha$ and $K\beta$ lines and the Bremsstrahlung radiation.

Table 2.1 A table of some characteristic X-ray lines.

Line	Energy (eV)	Width * (eV)
Y M ζ	132.3	0.47
Zr M ζ	151.4	0.77
Nb M ζ	171.4	1.21
Mg K α	1253.6	0.70
Al K α	1486.6	0.85
Si K α	1739.5	1.00
Y L α	1922.6	1.50
Zr L α	2042.4	1.70

* Defined as the full width at half maximum height of the line

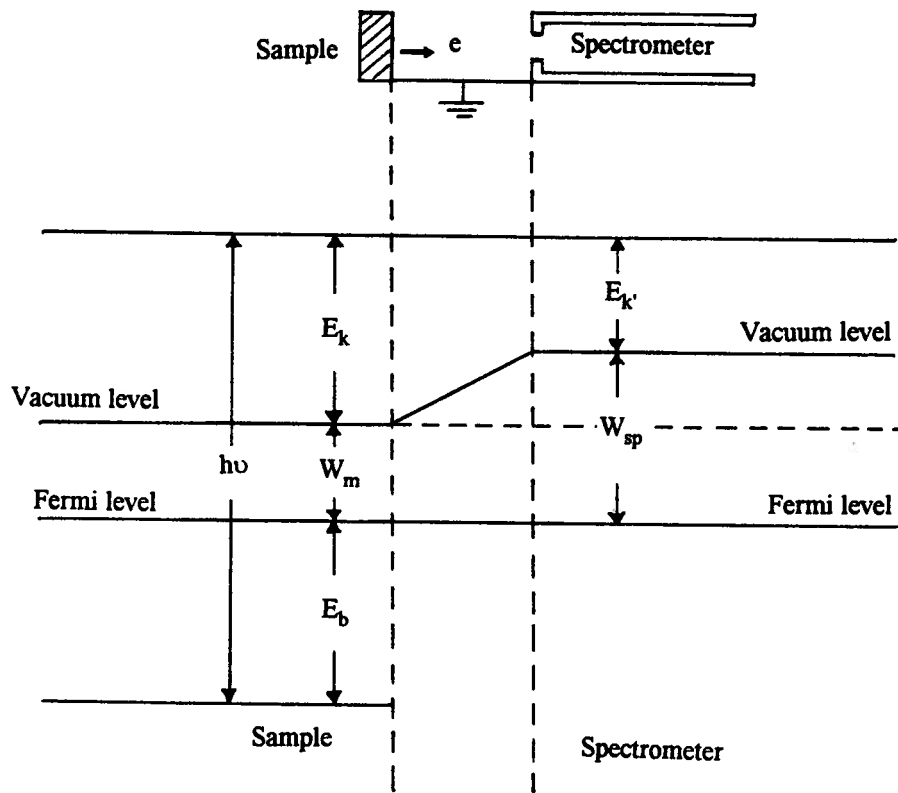


Figure 2.4 Reference levels for a metal sample and a spectrometer.

During XPS measurement, a metallic sample is in electrical contact with the spectrometer. Consequently, their Fermi levels are equal. However, their vacuum levels, and so their work functions, are not the same. The resultant kinetic energy (E_k') of a photoelectron measured in the spectrometer will be equal to:

$$E_k' = h\nu - E_b - W_{sp} \quad (2.3)$$

where W_{sp} is the work function of the spectrometer. W_{sp} is determined by calibrating with standard samples, and it is constant for different measurements as long as the spectrometer is not exposed to atmospheric pressure. A common reference photoelectron line for calibration is Au $4f_{7/2}$ at a binding energy of 84.0 eV.

In addition to the photoelectrons emitted from the above process, Auger electrons can also be emitted due to relaxation of the energetic ions left after the photoemission. In the Auger process, shown schematically in Figure 2.5, an electron from the L_1 shell falls into the inner K shell vacancy created by the initial X-ray irradiation; the energy released ($E_K - E_{L_1}$) is transferred to an electron in the $L_{2,3}$ shell, which is emitted as an Auger electron. The final state of the atom is doubly ionized. The kinetic energy ($E_{KL_1L_{2,3}}$) of this Auger electron is approximately equal to:

$$E_{KL_1L_{2,3}} = E_K - E_{L_1} - E_{L_{2,3}} \quad (2.4)$$

and this kinetic energy is basically a function of the atomic energy levels involved, so that measurements of the Auger energies from a surface give direct elemental identification. In XPS analysis, photon excited Auger electron spectra are frequently present, and can help the identification of chemical composition in the sample.

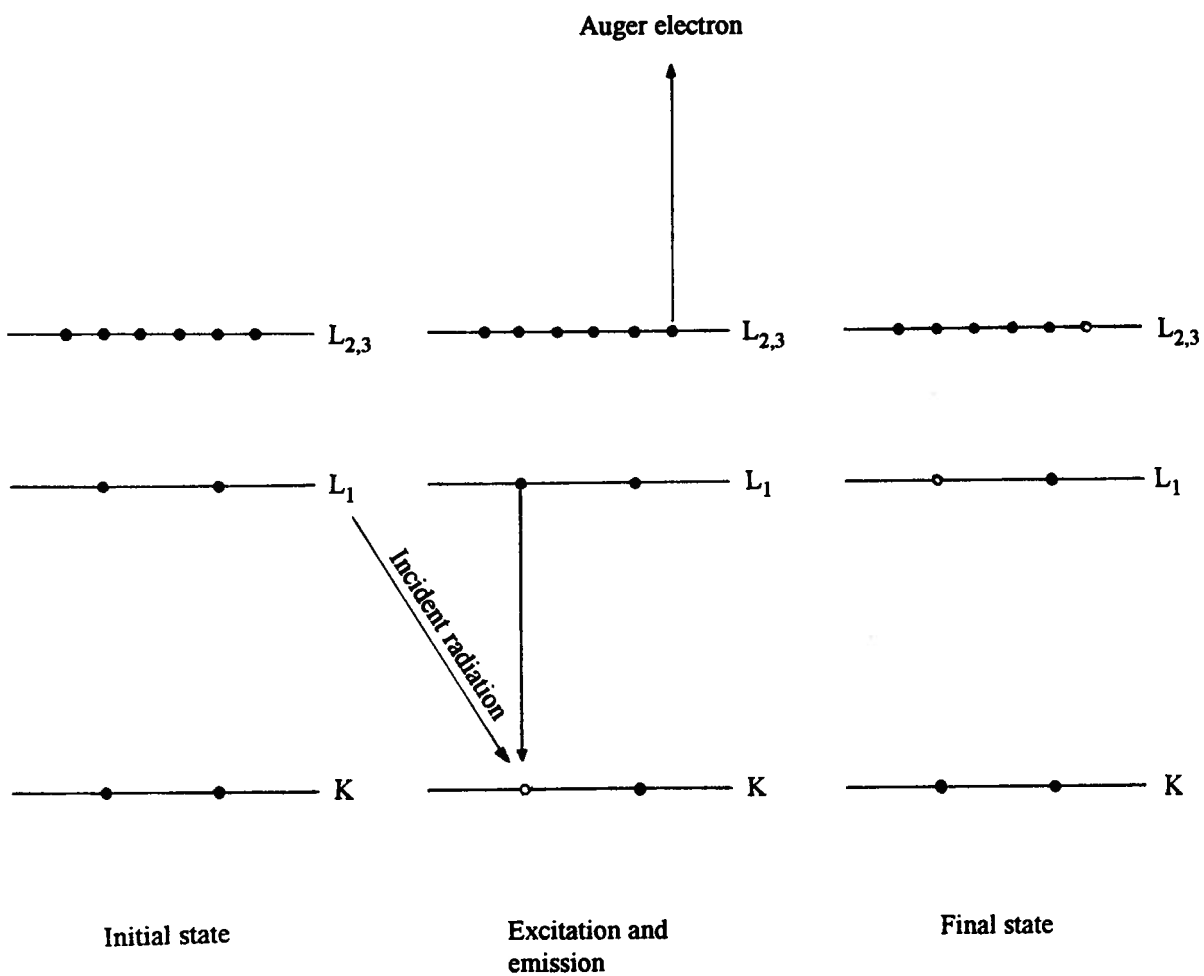


Figure 2.5 A schematic diagram of the Auger process.

(B) Surface Sensitivity of XPS

The reason why XPS is a surface sensitive analytical technique is related to the inelastic mean free path of electrons in the low energy range (e.g. 2 keV or less) in solids. Electrons in this energy range traveling through a material have a relatively high probability of experiencing inelastic collisions, therefore causing an energy loss. The inelastic mean free path (IMFP, λ) is defined as the average distance traveled by an electron without losing energy.

The intensity of electrons, I , traversed through a sample with thickness t , is equal to:

$$I = I^0 (1 - \exp(-t / \lambda)) \quad (2.5)$$

where I^0 is the intensity of electrons originated from the bulk. It is observed that 63% of the electron intensity will emanate from a depth of λ , 87% from a depth of 2λ , and 95% from a depth of 3λ . A common expression of the sampling depth in XPS is 3λ for the normal exit direction, that is the depth from which 95% of signal intensity arises.

λ is a function of the material and the electron energy. Calculations of λ have been made [2.8-2.11], and the compilation of experimental values by Seah and Dench [2.12] is given in Figure 2.6, in terms of atomic monolayers as a function of electron kinetic energy. For photoelectrons with kinetic energy between 100 to 1000 eV, λ typically ranges from about 2 to 8 monolayers. This ensures that the photoelectrons in a peak must originate close to the surface in order that they can escape into the vacuum and be detected without loss in energy. Strong inelastic scattering therefore gives XPS its surface sensitivity.

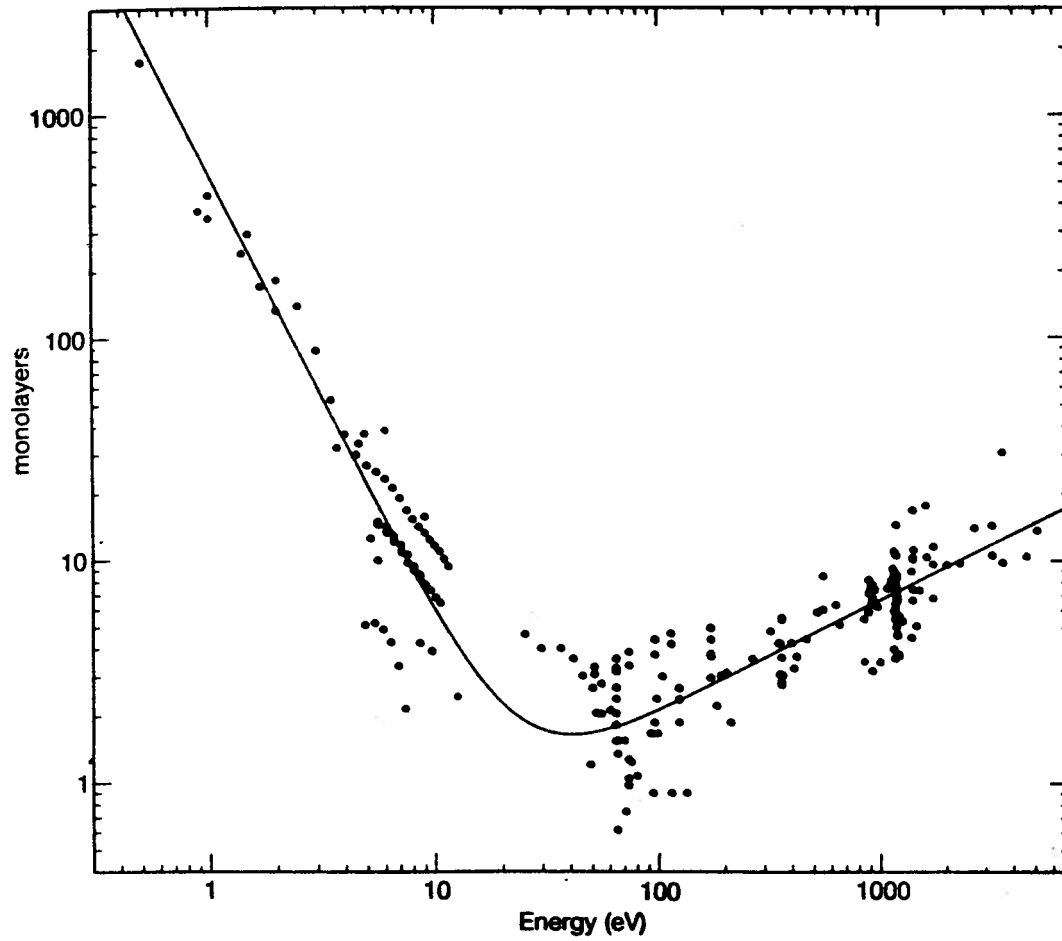


Figure 2.6 The compilation by Seah and Dench of measurements of the inelastic mean free path, λ , for different elements.

2.1.3 Chemical Analyses with XPS

(A) Qualitative Analysis

To characterize the surface chemistry of a sample under investigation, the first step to be taken is to identify the elements present. This is achieved by recording a survey or wide scan XPS spectrum. A typical survey scan spectrum of a copper sample excited by $MgK\alpha$ radiation is shown in Figure 2.7 [2.13]. Photoelectron peaks, arising from direct excitation of core-level electrons, are labeled with $2p_{1/2}$, $2p_{3/2}$, $3s$, and $3p$. In general, the core photoelectron peaks are the narrowest features in a XPS spectrum. Auger electron peaks in the LMM series are also indicated. Identification of these peaks can be made with the aid of data tabulated in Handbooks [2.13, 2.14].

In XPS spectra, peaks generally appear with an increasing background. In part this is due to photoemission by Bremsstrahlung radiation. In addition, the presence of a high binding energy tail is a consequence of electrons suffering energy loss during the interaction with the sample. This latter phenomenon causes the background in a XPS spectrum to have a stair-step appearance.

Photoelectron core peaks are labelled with the principal quantum number, n , (e.g. values 1, 2, 3, ...) and the angular momentum quantum number, l , (e.g. values 0, 1, 2, 3, or respectively called s, p, d, or f) (Table 2.2) [2.15]. A characteristic feature of the p, d, and f peaks is the spin-orbit splitting, for which Figure 2.8 [2.16] shows the example of the Zn $2p$ photoelectron peaks. The interaction of the spin and orbital electron motions results in two different energy levels, although this does not occur for s orbitals, which are symmetrical. The coupling effect is designated in XPS spectra by the subscripts $1/2$ and

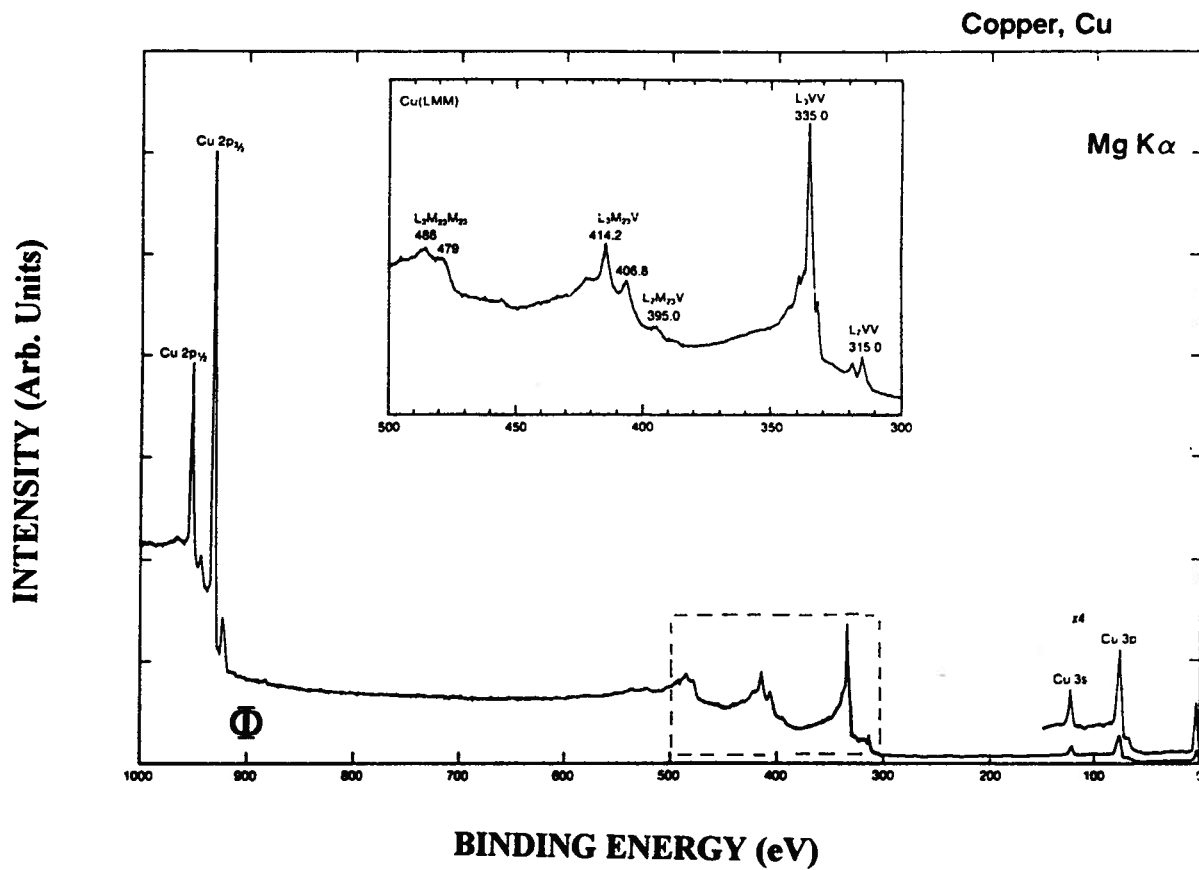


Figure 2.7 XPS survey scan spectrum of copper, with an insert of the Cu LMM Auger series.

Table 2.2 A summary of the atomic orbital nomenclature.

Principal quantum number (n):	1, 2, 3, 4, 5,
	K, L, M, N, O,
Angular momentum quantum number (l):	0, 1, 2, 3,
	s, p, d, f,
Subscript:	$l + 1/2$ or $l - 1/2$
Example:	$2 p_{1/2}$, $2 p_{3/2}$

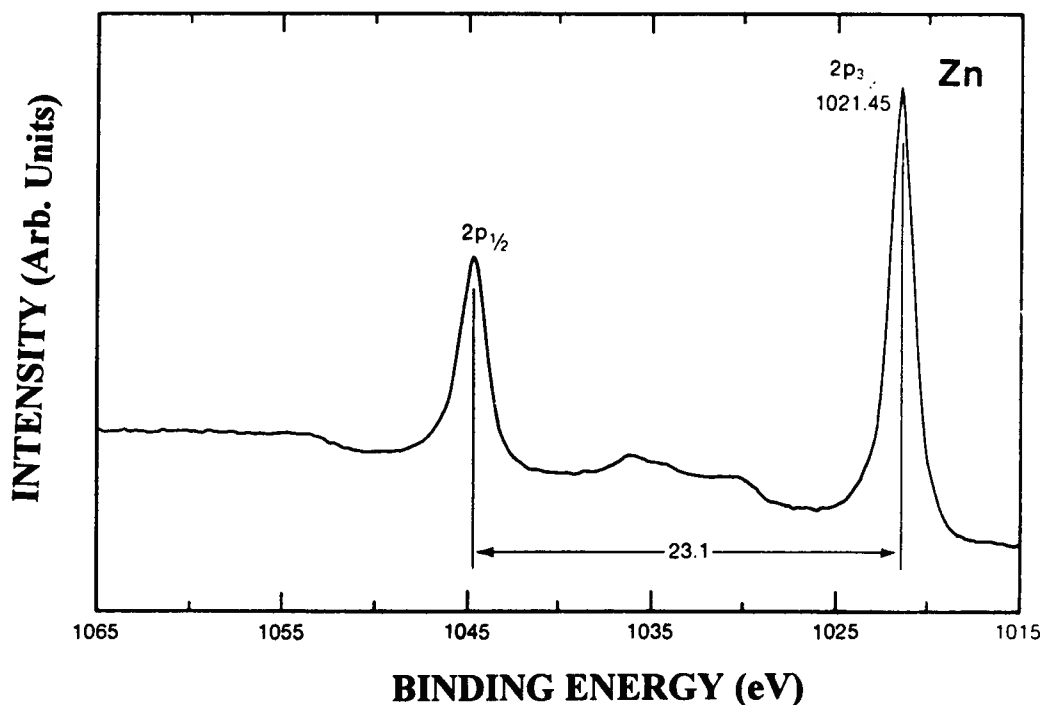


Figure 2.8 Spin-orbit splitting for the Zn 2p photoelectron peaks.

3/2 for p orbitals, 3/2 and 5/2 for the d orbitals, and 5/2 and 7/2 for f orbitals; the peak intensity ratios are 1:2, 2:3 and 3:4 respectively.

Chemical bonding or chemical state information for a particular element can be obtained from high-resolution spectra. Figure 2.9 shows a high resolution spectrum of Al 2p photoelectron peaks from an aluminum alloy with a naturally formed oxide layer. The two Al 2p peaks result from different chemical environments; that at 71.5 eV is identified as metallic aluminum, while that at 74.1 eV is identified as aluminum oxide. This change in binding energy is a chemical shift effect, whereby the binding energies of the inner core electrons are influenced by changes in the valence electron environment. The higher binding energy peak is assigned to the oxide because of the net positive charge in those aluminum atoms which are bonded to oxygen. The reduced electrostatic shielding results in these Al 2p electrons being more strongly attracted to the nucleus, and so a higher binding energy is observed for this Al 2p photoelectron peak.

On the other hand, a possible error in identification of a peak position may result from any electrostatic charging of a poor conductive sample. It is noteworthy that charging effects occur with Auger electron lines, as well as with photoelectron lines, and the use of the Auger parameter (α) [2.17] can help minimize possibilities for mistaking an artificially induced shift in binding energy from charging as being due to a chemical shift dependent on chemical environment. The Auger parameter can be defined as:

$$\alpha = E_{ka} - E_{kp} \quad (2.6)$$

where E_{ka} is the kinetic energy of an appropriate Auger electron peak from a particular atom, and E_{kp} is the kinetic energy of a photoelectron from the same atom. Since the values of E_{ka} and E_{kp} have a common reference energy, measured values of the Auger

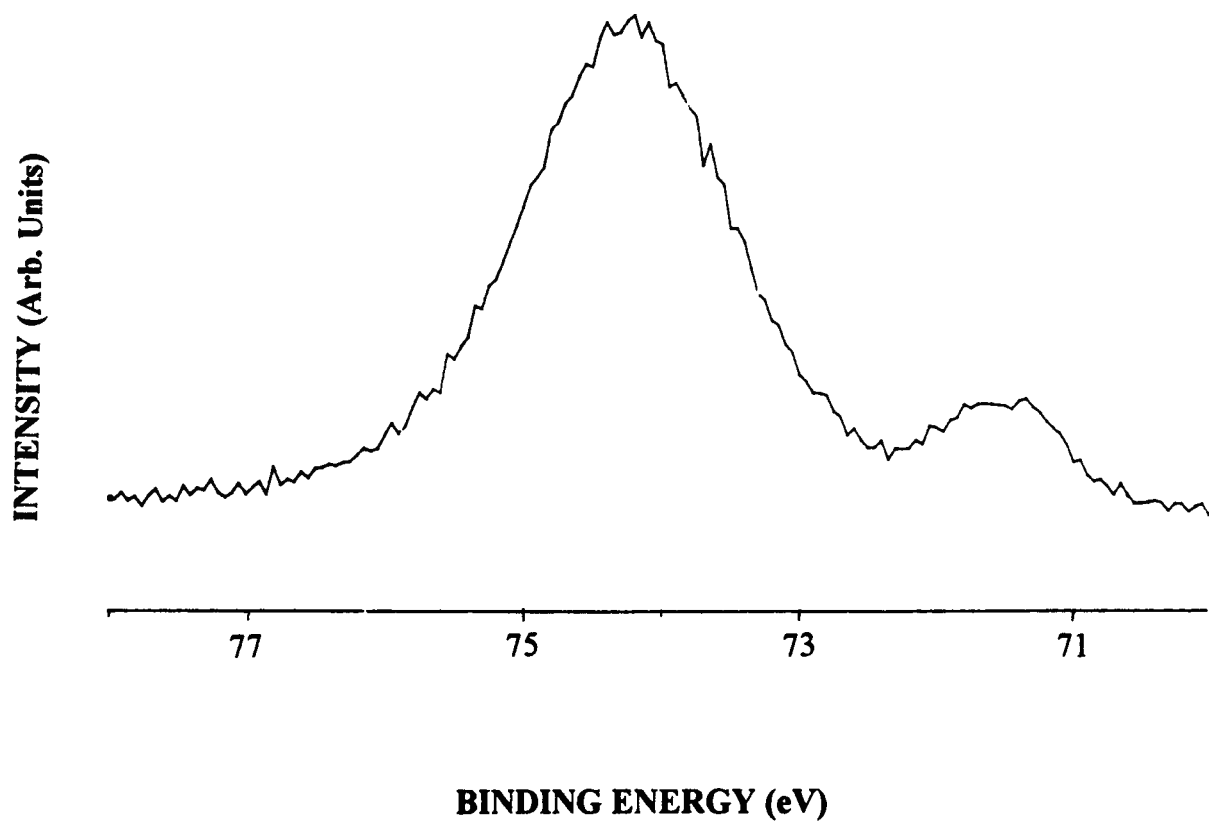


Figure 2.9 High resolution XPS spectrum of the Al 2p photoelectron peak from an aluminum alloy with naturally formed oxide layer.

parameter should be independent of any electrostatic charging of the sample. A table of this parameter for zinc compounds is shown in Table 2.3 [2.14]. Conventionally, the sum of the excitation source energy ($h\nu$) and the Auger parameter is used for comparison. From the table, it is shown that the measured binding energies of the Zn $2p_{3/2}$ photoelectrons for zinc and zinc oxide are both at the value of about 1022 eV. Therefore, by only comparing the binding energies, it is impossible to distinguish their differences. However, if their Auger parameters are taken into consideration, the sums of the excitation energy and Auger parameter for zinc (at 2013.9 eV) and zinc oxide (at 2010.0 eV) provide a better identification for their chemical states.

(B) Quantitative Analysis

The area of a photoelectron peak defines the peak intensity. For a homogeneous sample, the number of photoelectrons emitted per second (I) can be expressed by [2.18]:

$$I = n f \sigma \theta y \lambda A T \quad (2.7)$$

where n = number of appropriate atoms per unit volume of the sample (cm^{-3})

f = the X-ray flux ($\text{cm}^{-2}\text{sec}^{-1}$)

σ = photoelectric cross-section for the atomic orbital (cm^2)

θ = an angular efficiency factor for the instrumental arrangement based on the angle between the photon path and detected electron

y = efficiency in the photoelectric process for the formation of photoelectrons

λ = inelastic mean free path of the photoelectrons in the sample (cm)

Table 2.3 The Auger parameters for zinc compounds.

Compound	$2p_{3/2}^{\dagger}$	$L_3M_{45}M_{45}^{\dagger}$	$\alpha + h\nu^*$
Zn	1021.7	992.2	2013.9
ZnOx	1021.8	988.2	2010.0
ZnF ₂	1022.4	986.7	2009.1
ZnBr ₂	1023.2	987.5	2010.7

\dagger Binding energy of Zn $2p_{3/2}$ photoelectrons (in eV)
 Kinetic energy of the Auger LMM electrons (in eV)

* $h\nu = 1253.6$ eV (MgK α excitation source)

A = area of a sample from which photoelectrons are detected (cm²)

T = detection efficiency for electrons emitted from a sample

For given instrumental conditions, and a given photoelectron peak, the factors f , σ , θ , y , λ , A and T can all be grouped into the atomic sensitivity factor S. Then equation 2.7 can be re-expressed as:

$$n = I / S \quad (2.8)$$

and this allows the relative concentrations of the various constituents in a sample to be determined from:

$$C_x = n_x / \sum n_i = (I_x / S_x) / (\sum I_i / S_i) \quad (2.9)$$

Values of sensitivity factors are generally available for photoelectron peaks relative to the fluorine 1s peak as standard. In the work reported in this thesis, using the MAX 200 spectrometer, the sensitivity factors used were those provided by the manufacturer.

2.1.4 Angle Dependent XPS

Angle dependent XPS (ADXPS) can provide information on composition with depth for a material. The surface enhanced composition is emphasized for small take-off angle θ , as illustrated in Figure 2.10. The sampling depth t (introduced on p. 21) can now be extended to $3\lambda \sin \theta$. Therefore, the surface sensitivity is greater for smaller take-off angles.

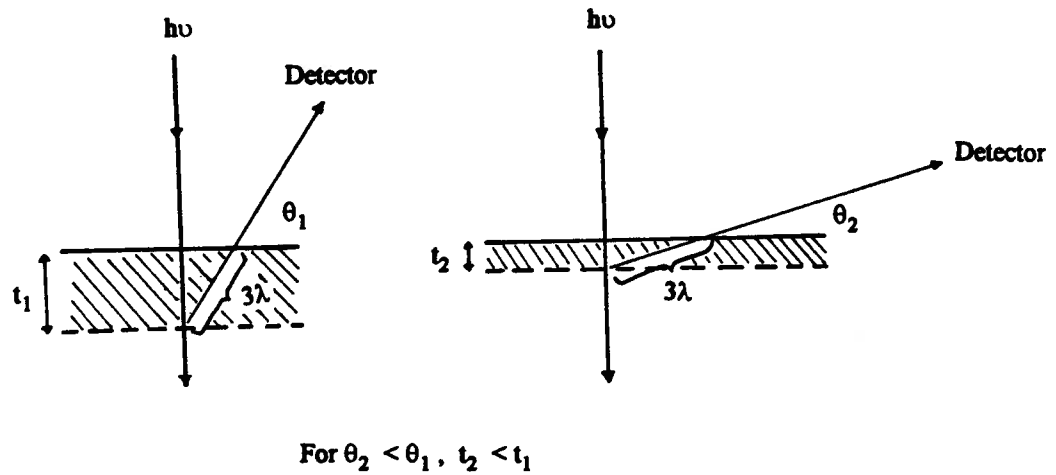


Figure 2.10 Illustration of the principle of angle dependent XPS (ADXPS).

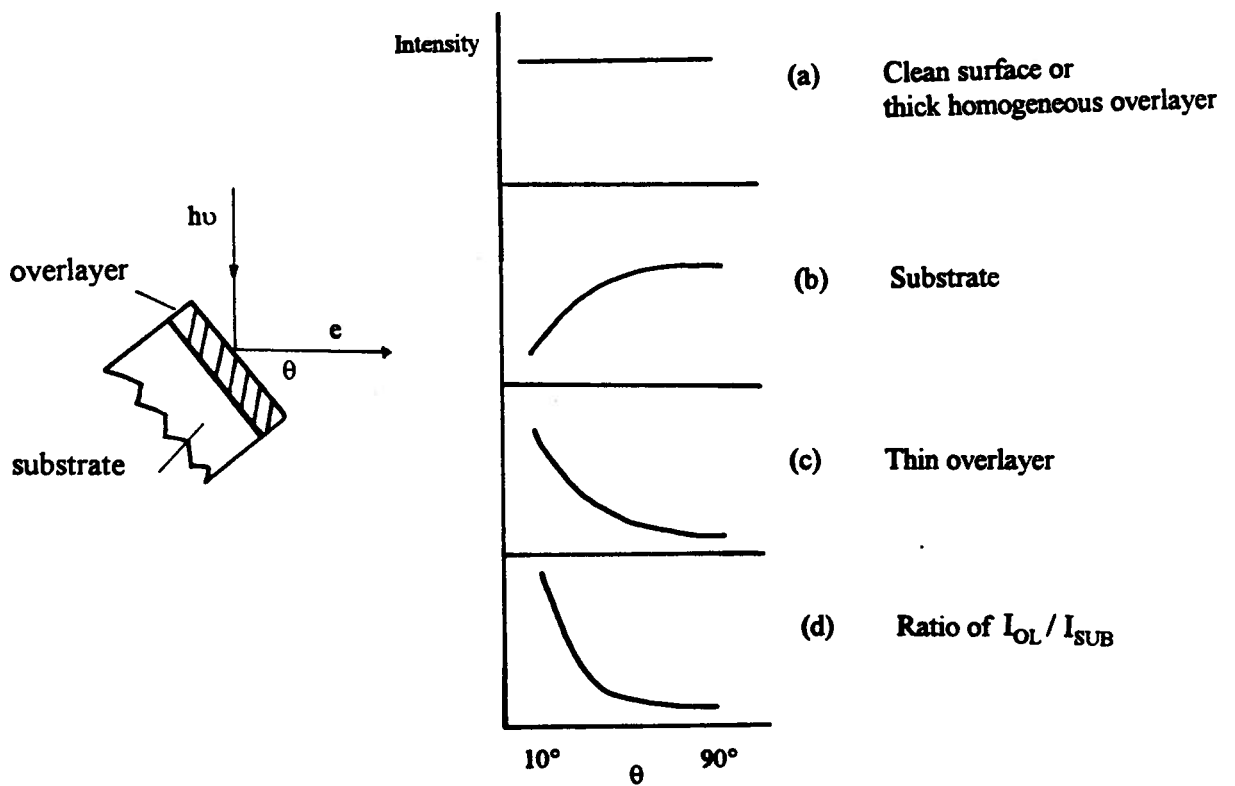


Figure 2.11 Theoretical angular dependent curves for a flat clean surface coated with an overlayer.

In a practical situation, a sample is often coated with an overlayer on top of a substrate material (Figure 2.11) [2.19]. In this case, the angular variations of intensities from the substrate, I_{SUB} , and the overlayer, I_{OL} , with thickness d , are given by:

$$I_{\text{SUB}} = I_{\text{SUB}}^{\circ} \exp(-d / \lambda_s \sin \theta) \quad (2.10)$$

$$I_{\text{OL}} = I_{\text{OL}}^{\circ} [1 - \exp(-d / \lambda_o \sin \theta)] \quad (2.11)$$

where λ_s and λ_o are the inelastic mean free paths of the substrate and overlayer materials, respectively. In the ideal situation, where the overlayer is homogeneous and flat, the above equations lead to curves of the types shown in Figure 2.11. For a clean surface (Figure 2.11(a)), or for a surface with an overlayer with thickness larger than about $3\lambda_o$, the intensity will be angle independent. For a sample covered with a thin overlayer (Figure 2.11(b) & (c)), the intensity from the substrate will increase with θ ; while the intensity from the overlayer will decrease with θ . Their ratio (Figure 2.11 (d)), $I_{\text{OL}} / I_{\text{SUB}}$, shows a more rapid decay with increasing θ . Actually, this ratio, $I_{\text{OL}} / I_{\text{SUB}}$, is useful to determine the thickness of an overlayer. If λ_s and λ_o are equal, then,

$$I_{\text{OL}} / I_{\text{SUB}} = I_{\text{OL}}^{\circ} / I_{\text{SUB}}^{\circ} [\exp(d / \lambda \sin \theta) - 1] \quad (2.12)$$

$$R(\theta) = K [\exp(d / \lambda \sin \theta) - 1] \quad (2.13)$$

$$[R(\theta) / K + 1] = \exp(d / \lambda \sin \theta) \quad (2.14)$$

$$\ln [R(\theta) / K + 1] = d / \lambda \sin \theta \quad (2.15)$$

where $R(\theta) = I_{\text{OL}} / I_{\text{SUB}}$ and $K = I_{\text{OL}}^{\circ} / I_{\text{SUB}}^{\circ}$.

Since the values of $R(\theta)$ and K can be obtained experimentally, the thickness of the overlayer, d , can be determined from the slope of a graph with $\ln [R(\theta) / K + 1]$ plotted against $1/\sin \theta$.

2.1.5 Bias Technique Applied on XPS

If a sample has some regions which are not in good electrical contact with the spectrometer, differential charging may occur, and this can give rise to misleading binding energy information about the chemical states of elements if care is not taken. This is because photoelectrons emitted from these regions have to overcome an extra potential resulting from this charging effect; thus the measured binding energy of these photoelectrons will become higher. However, recent work by Leung *et al* [2.20], following a study by Pertsin and Pashunin [2.21], suggests that components at a polymer-metal interface which are not in good electrical contact with the spectrometer can be distinguished by applying a bias potential. Figure 2.12 shows the Zn $2p_{3/2}$ photoelectron spectra from a zinc phosphate treated aluminum alloy surface. Curve 1 is obtained from the grounded sample. The presence of two components, at 1026.7 eV and 1023.3 eV, of this photoelectron peak implies that either the treated sample has two chemical states of zinc, or some areas of the sample suffered differential charging. Curve 2 shows the result of shifting the spectrum back by 94 eV after measuring with negatively biased potential (-94 V) applied on the sample. Only the 1023.3 eV component is observed in curve 2, and it is present in both curves. This suggests that the chemical component giving rise to it is not subject to differential charging, but that component at 1026.7 eV, which only appears in curve 1, is not in good electrical contact with the metal and thus becomes changed by the bias potential in an uncontrolled way so that it does not appear in curve 2.

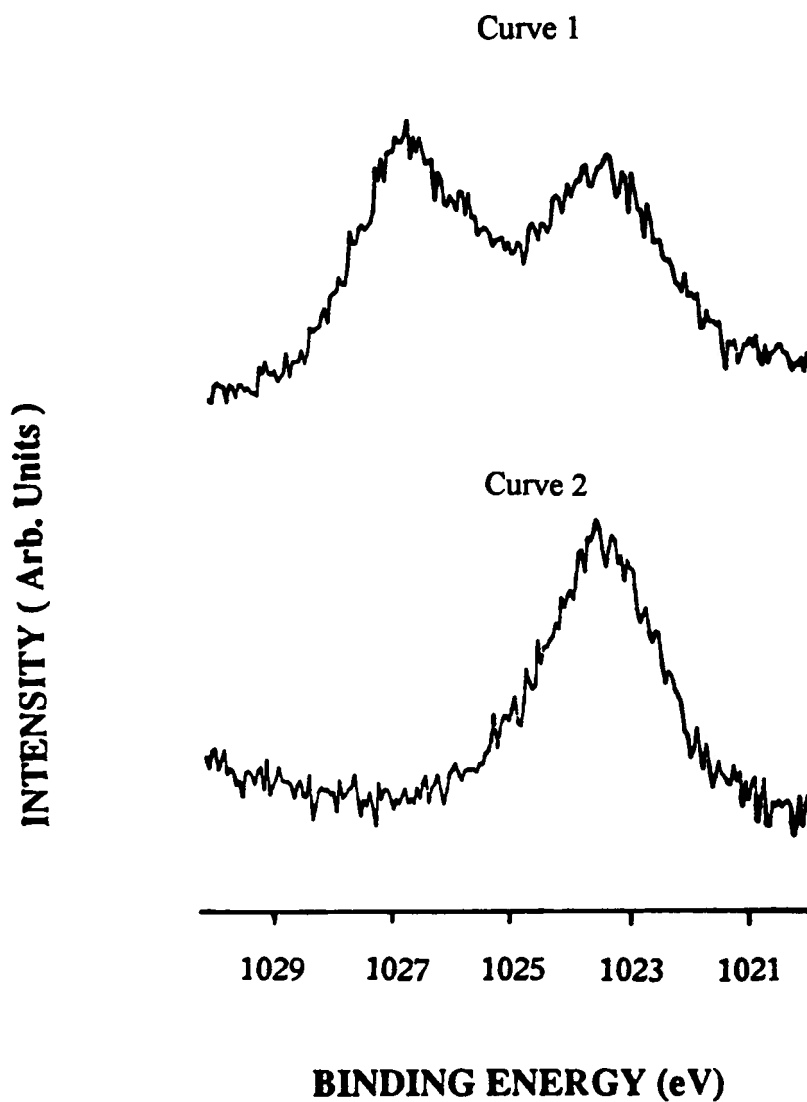


Figure 2.12 Zn 2p_{3/2} photoelectron peaks from a zinc phosphate treated aluminum sample. Curve 1 is obtained from the grounded sample. Curve 2 is obtained from the sample with -94 V biased potential applied on the sample and shifted back by 94 eV after measuring.

2.1.6 Instrumentation of XPS

The XPS measurements made in this work were obtained with a Leybold MAX 200 spectrometer [2.22] which is shown schematically in Figure 2.13. This spectrometer consists of three vacuum chambers, including a transfer chamber, an analysis chamber and a preparation chamber. The latter two are maintained for ultra high vacuum conditions but the analysis chamber (Figure 2.14) is where the XPS measurements are performed. Major components in the analysis chamber include a dual anode X-ray source, a concentric hemispherical analyzer with a multichannel detector, and 5-motion manipulator with sample holding, heating and cooling. In addition, this chamber also contains an ion gun for sputtering and ion scattering spectroscopy (ISS), an X-ray monochromator for increased energy resolution, and an electron flood gun to aid studies on insulating samples. Further discussion of some of these components is included in the following sections. The preparation chamber was not used in the present work, and the transfer chamber is used for sample entry.

(A) Ultra-High Vacuum

The photoelectron spectrometer is operated in the ultra-high vacuum (UHV) [2.23] range of 10^{-8} to 10^{-10} torr. In such a vacuum condition, the emitted electrons can reach the energy analyzer without being significantly scattered by the residual gas molecules. As mentioned before, most photoelectrons analyzed originate from the outermost atomic layers. As a result, the technique is very sensitive to surface contamination. Since many experiments need an atomically clean sample surface, and sometimes very small amounts of contaminant can affect an experiment significantly, it is necessary to operate under conditions in which the accumulation of contamination is

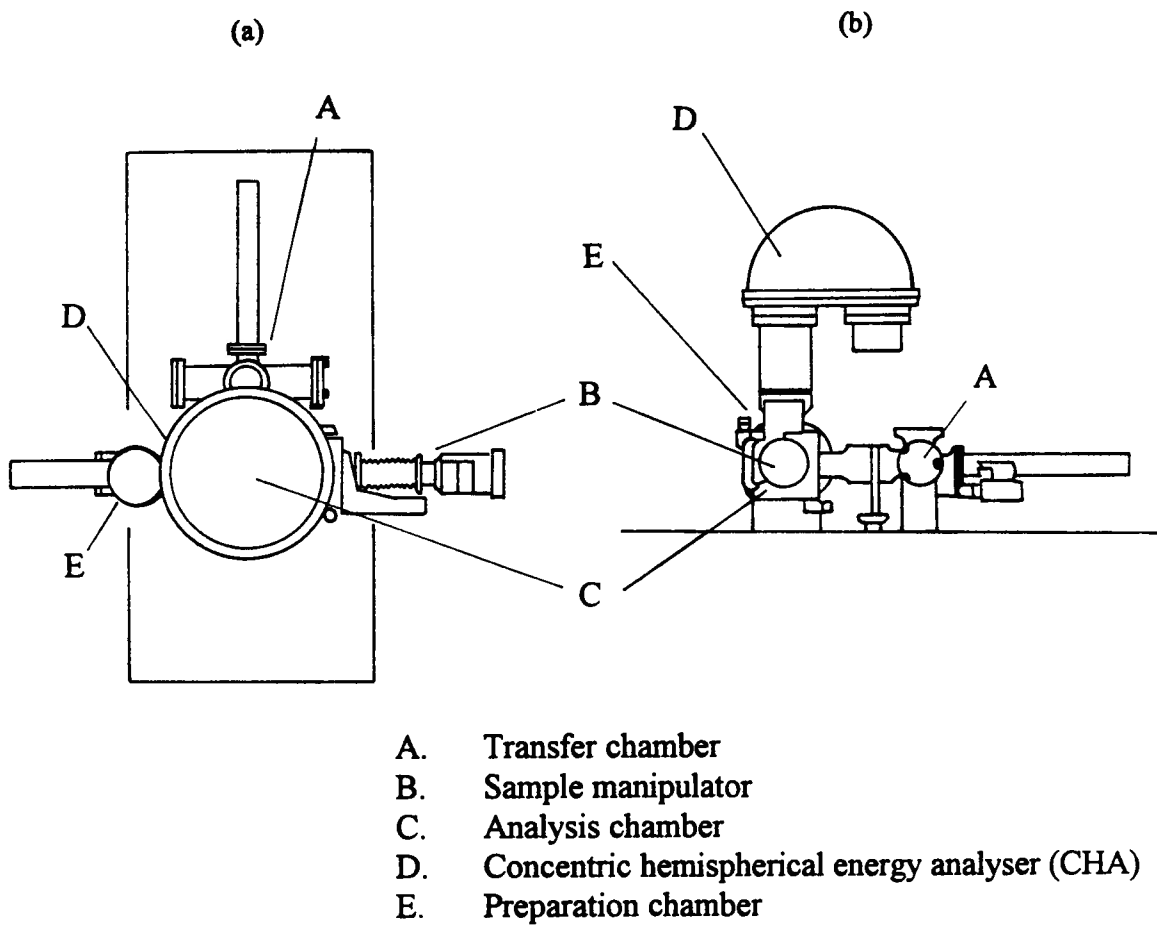


Figure 2.13 A schematic indication of the Leybold MAX 200 spectrometer (a) top view (b) side view.

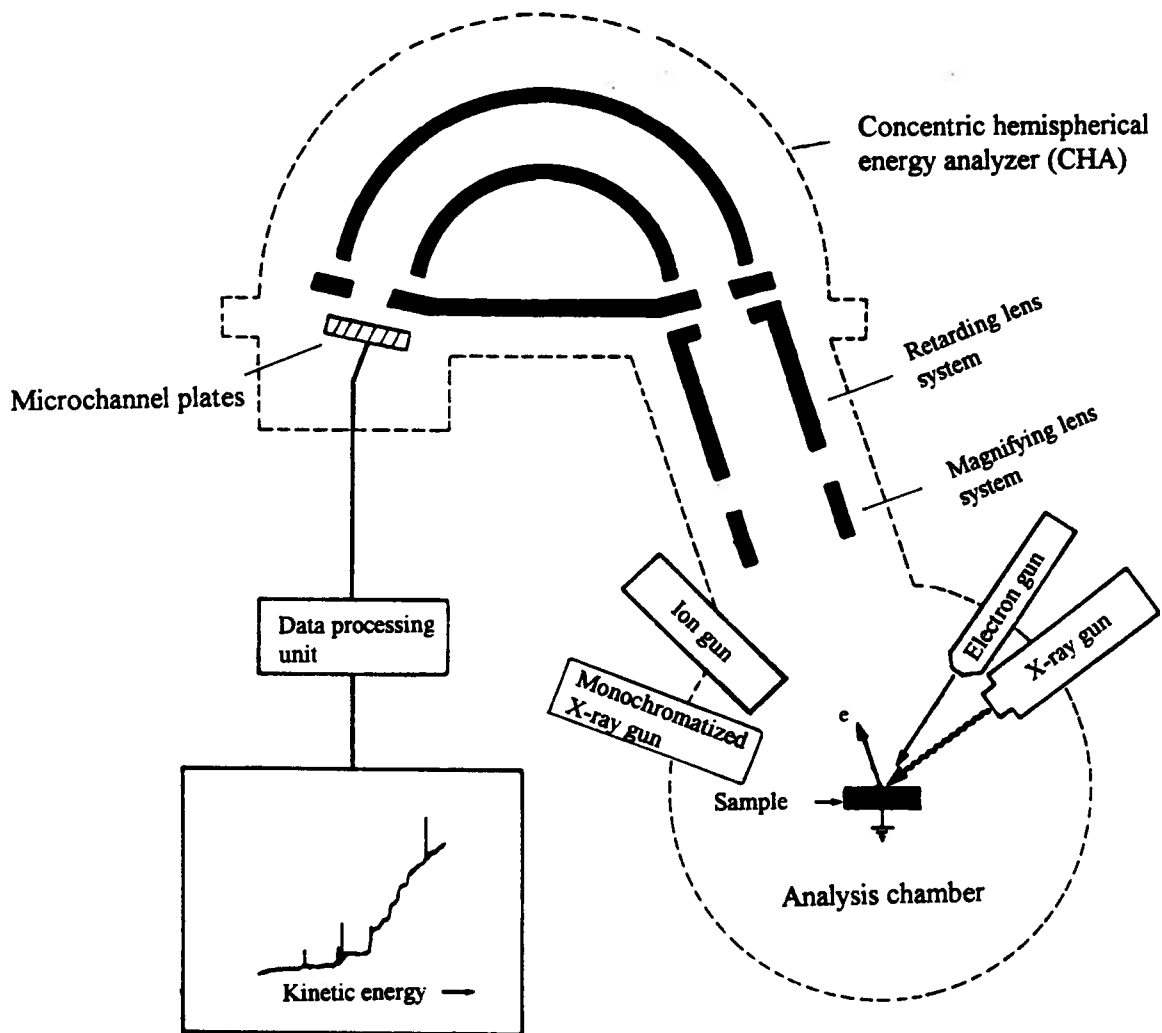


Figure 2.14 Components of the MAX 200 analysis chamber.

negligible during an experiment. At a pressure of 10^{-5} torr, it is possible for a monolayer of gas to be adsorbed onto a surface in about one fifth of a second, if every collision sticks. Therefore, to ensure that no more than about 0.05 atomic layers of contaminant accumulates during data acquisition (say 30 minutes), pressure as low as 10^{-10} torr is required.

The chambers and the associated piping of the spectrometer are constructed from stainless steel. The preparation, transfer and analysis chambers are initially rough pumped to the 10^{-2} torr range by rotary pumps, then pumped to the 10^{-7} or 10^{-8} torr range by the tubomolecular pumps, finally UHV can be achieved in the analysis chambers by baking at around $140\text{ }^{\circ}\text{C}$ for 12 hours or more while pumping. Baking removes adsorbed gas from the chambers walls so that UHV can be achieved within a reasonable time, after cooling back to room temperature. Figure 2.15 shows the pumping system used in the MAX 200 spectrometer; an additional ion pump is used for the X-ray source system.

For sample entry, the transfer chamber is vented with nitrogen at atmospheric pressure, and after closing, the chamber is pumped down to 10^{-8} torr. The samples are then transferred into the analysis chamber. The whole sample transferring process is efficient and maintains the UHV condition in the analysis chamber.

(B) Excitation Source

A dual anode [2.23] X-ray source was used in this research; it has aluminum and magnesium deposited on different faces of the anode block. Thus, the excitation source can be changed by simply switching the anode filaments. Typically, an accelerating potential of 15 kV is used for the production of $\text{MgK}\alpha$ and $\text{AlK}\alpha$ radiation, while simultaneously, the anode is cooled by a deionized water system (Figure 2.16).

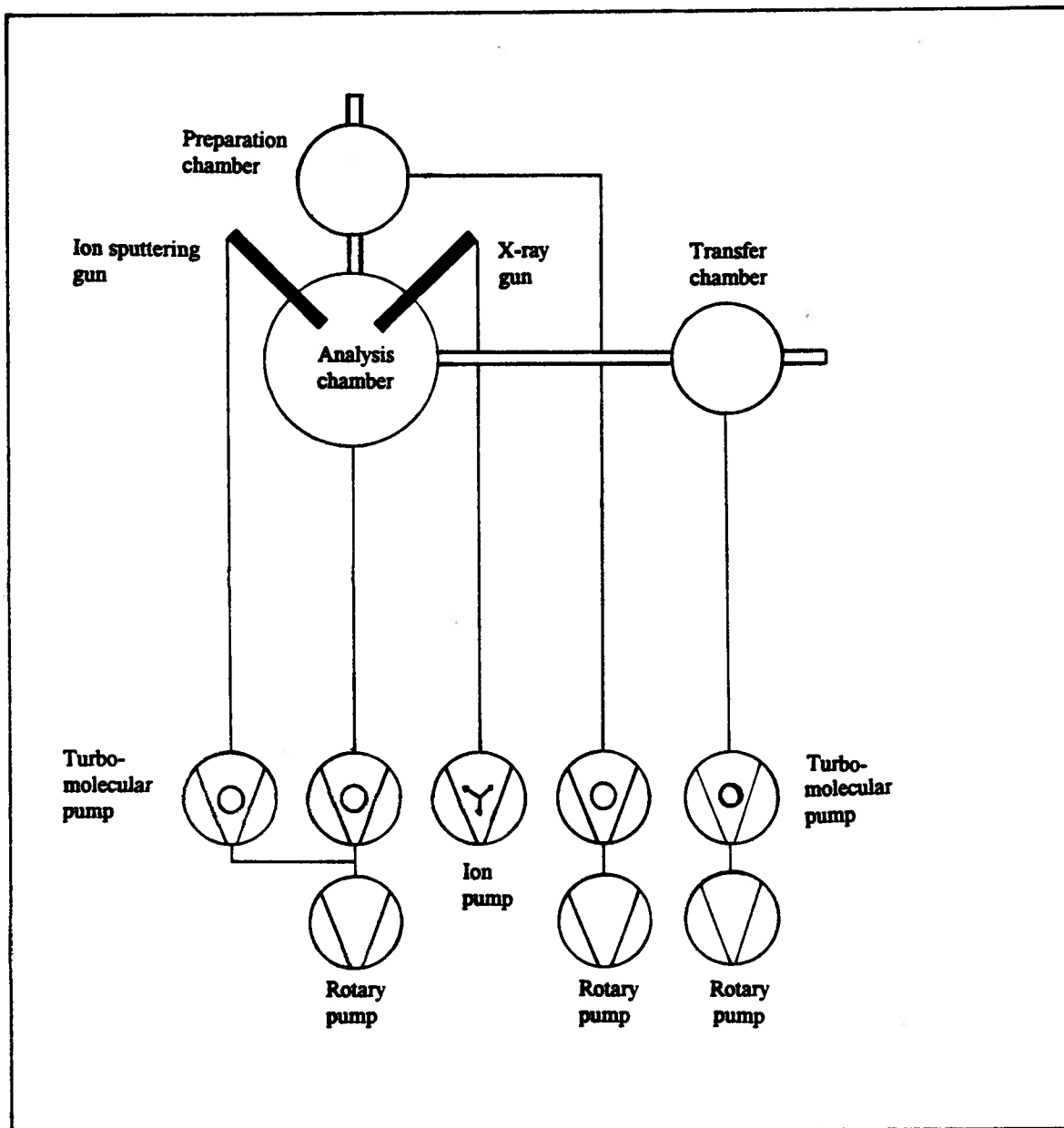


Figure 2.15 The pumping system of the XPS spectrometer.

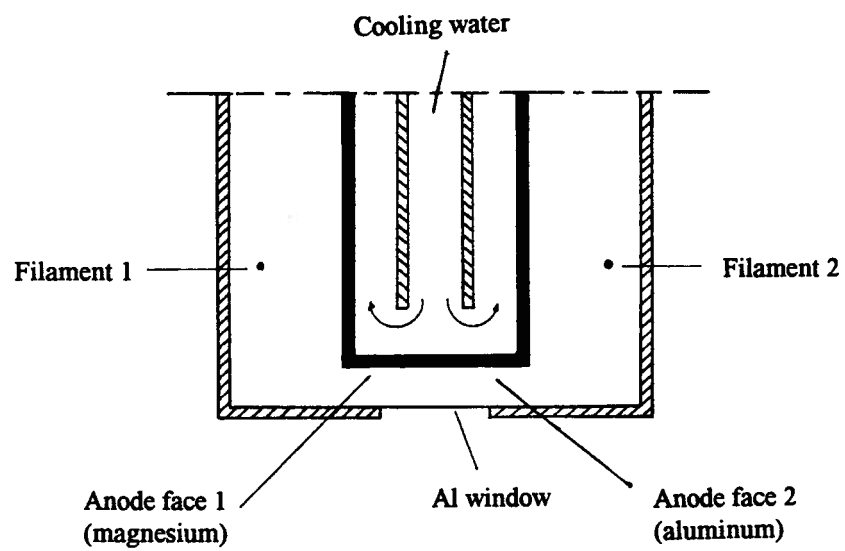


Figure 2.16 A schematic diagram of the Al and Mg dual anode X-ray source.

An aluminum foil window, of thickness about 2 μm , is positioned between the anode and sample to prevent stray electrons, radiative heating, and contamination from the anode region reaching the sample. This window material is transparent to $\text{MgK}\alpha$ and $\text{Al K}\alpha$ radiation, and is sufficiently thin that the X-ray flux is not significantly attenuated.

(C) Sample Handling

In the MAX 200 system, up to seven sample holders can be locked on to the sample magazine, prior to introducing into the transfer chamber. One sample holder is transferred at a time to the analysis chamber by the lock rod, and then locked on to the manipulator. The manipulator allows three linear degrees of movement for the sample (x , y , and z), as well as two rotational variables, θ and ϕ , to give proper sample positioning and angle dependent measurements. Figures 2.17 and 2.18 show this sample handling assembly.

(D) Electron Energy Analyzer

In the MAX 200 system, the photoelectron kinetic energies are measured with a concentric hemispherical analyzer (CHA) [2.23], which is coupled with an entrance retarding lens system. Figure 2.19 [2.24] shows a schematic diagram of the CHA component. The CHA consists of two concentric hemispheres of radii R_1 (inner) and R_2 (outer). A deflecting potential ΔV is applied between the spheres so that the outer is negative and the inner is positive. The entrance slit (with width ω_1) and exit slit (with width ω_2) are centered on the mean radius R_0 , where $R_0 = (R_1 + R_2) / 2$. For the ideal situation, where an electron (charge e , and kinetic energy E_0), is travelling on the circular orbit of radius R_0 , the relationship between E_0 and the

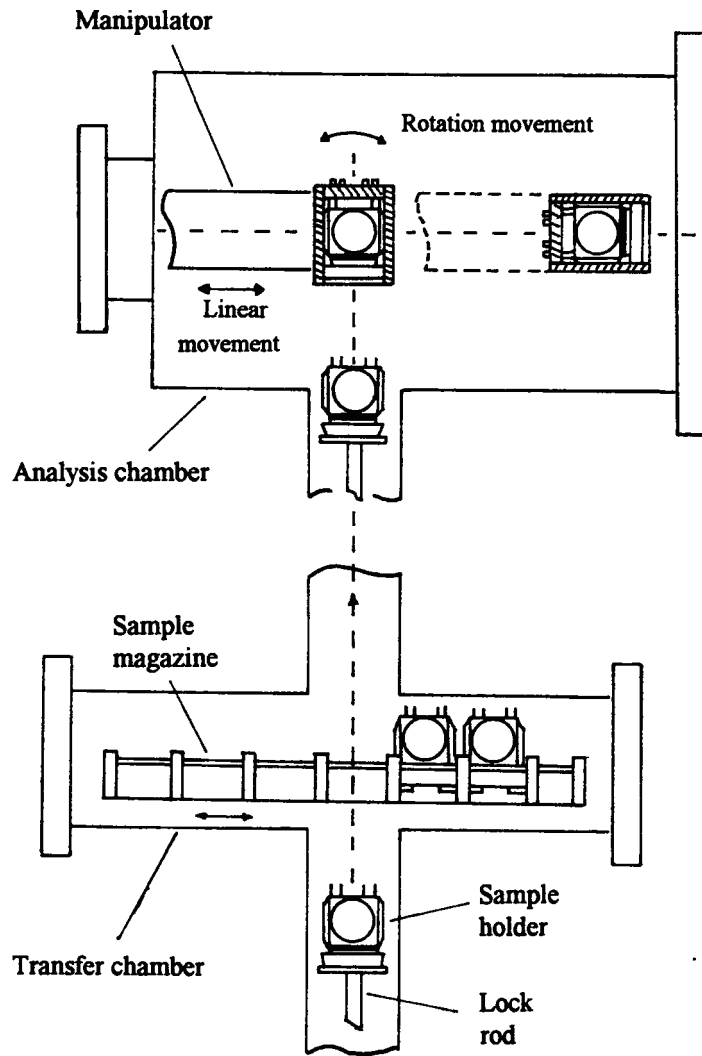


Figure 2.17 The MAX 200 system: sample handling assembly.

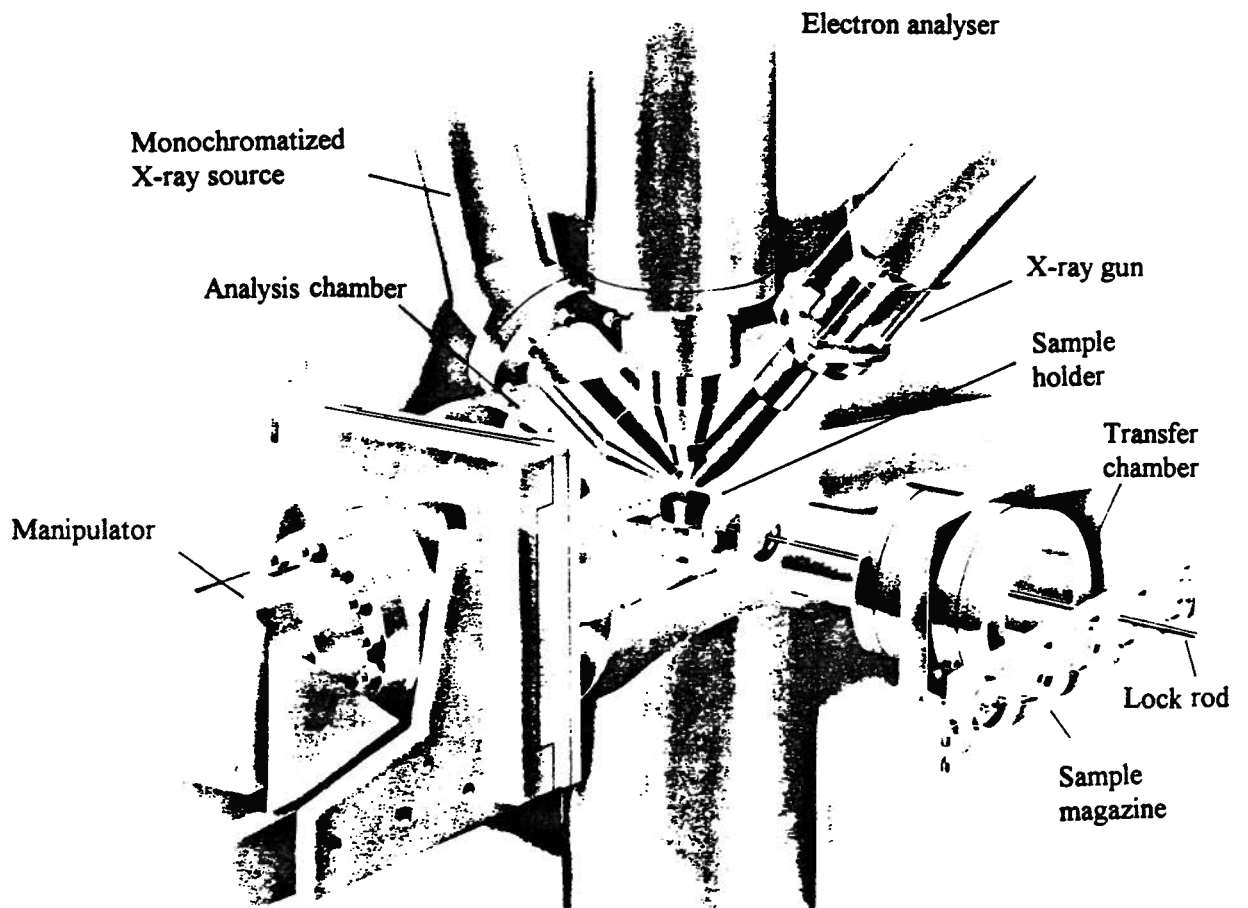


Figure 2.18 The analysis and transfer chambers of the spectrometer in MAX 200 system.

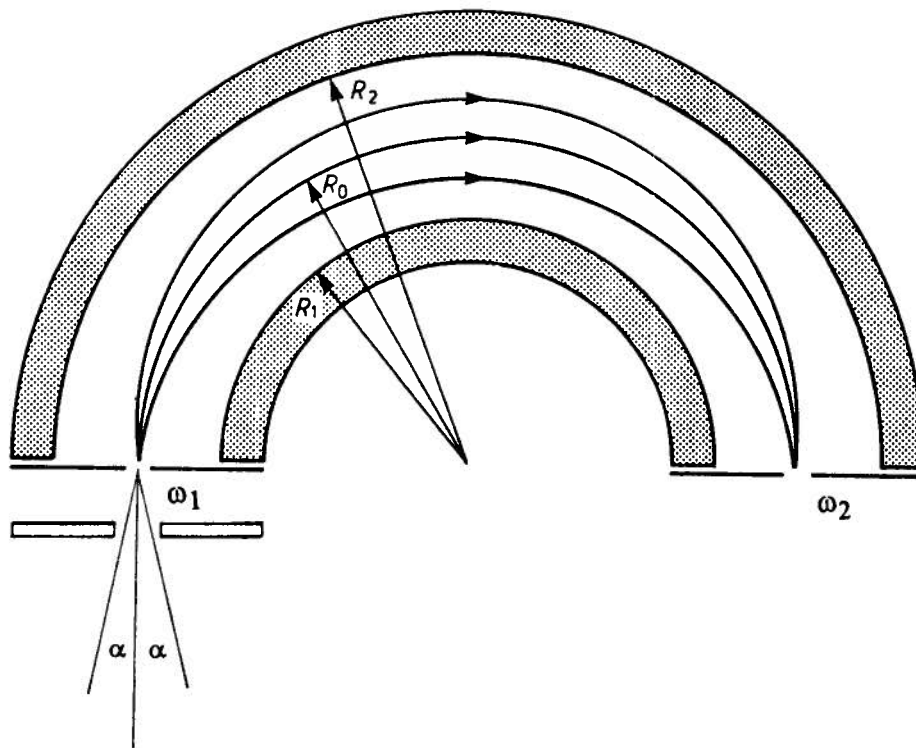


Figure 2.19 A schematic diagram of a concentric hemispherical analyzer (CHA).

deflecting potential is:

$$e\Delta V = E_0 (R_2 / R_1 - R_1 / R_2) \quad (2.16)$$

to ensure the electrons pass through the exit slit of the analyzer. Suppose that the divergence of electrons entering the analyzer from the ideal path is α , the relative resolution of the concentric hemispherical analyzer is given by:

$$\Delta E_{\text{spec}} / E_0 = (\omega_1 + \omega_2) / 2 R_0 + \alpha^2 \quad (2.17)$$

where ΔE_{spec} is the energy resolution. Since ω_1 , ω_2 , R_0 and α are restricted by the spectrometer construction, the relative resolution of the spectrometer varies with the pass energy E_0 . Therefore, the smaller the E_0 , the better the resolution.

In order to perform a highly precise energy analysis under a constant resolution condition, electrons entering the analyzer are pre-retarded by the lens system to a fixed kinetic energy, called the pass energy (E_0). The kinetic energy scanning is done during the pre-retardation process, where the applied voltage in the lens system keeps ramping so the kinetic energies of electrons are retarded to the energy equal to E_0 and able to pass through the analyzer. Electrons with higher or lower kinetic energy than the pass energy will be deflected and hit the walls of the analyzer; thus are unable to reach the detector.

The experimental resolution for a photoelectron peak, defined as the full width at half maximum (FWHM), in a XPS spectrum is actually determined by three basic factors namely ΔE_{source} , the peak width for the X-ray source, ΔE_{spec} , the analyzer resolution and ΔE_{atom} , the natural width determined by the uncertainty principle for the lifetime of the

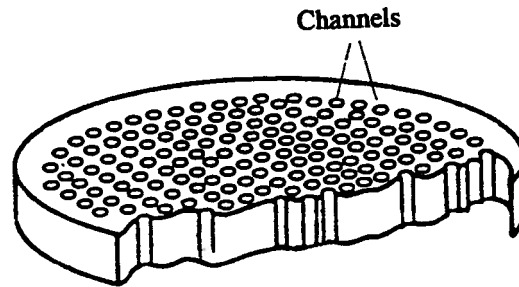
ionic core state. For the assumption that the peaks have a Gaussian line shape, the measured half width is given by:

$$\Delta E_{\text{total}} = (\Delta E_{\text{source}}^2 + \Delta E_{\text{spec}}^2 + \Delta E_{\text{atom}}^2)^{1/2} \quad (2.18)$$

(E) Detector

Electrons which exit the hemispherical analyzer are detected by the microchannel plates (Figure 2.20 [2.25]). Each electron impacting on this detector results in a electron pulse in a channel with a multiplication of around 10^7 . These pulses are transformed into electrical signals and processed by the computer. The MAX 200 system in our laboratory is interfaced to a HP 1000 based microprocessor using Data System DS 100 software and is connected to the display unit.

(a)



(b)

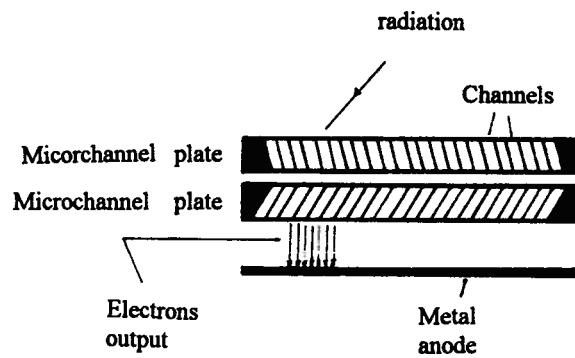


Figure 2.20 (a) A cutaway view of a microchannel plate, (b) a schematic diagram of a microchannel plate assembly.

2.2 Scanning Electron Microscopy

2.2.1 Background

Because of its high resolution and extensive magnification range, scanning electron microscopy (SEM) [2.26] has unique capabilities for analyzing surfaces. Unlike the reflected light microscope, which forms an image from light reflected from a sample surface, SEM uses electrons for surface imaging. Actually, the wavelength of the radiation source determines the resolution levels. Higher energy electrons have shorter wavelengths and are thus capable of generating higher-resolution information. Enhanced resolution permits higher magnification without loss of detail. Generally, the maximum resolution and magnification limits of conventional light microscopes are 2000Å and 2000 times; whereas the limits of conventional SEM are 40Å and 75000 times, respectively.

A basic SEM unit consists of four main components: the illuminating / imaging system, the information system, the display system and the vacuum system. Each of these systems and their relationships are discussed below. In our work, a Hitachi S-2300 model scanning electron microscope is employed. Micrographs are taken at 4000 magnification with 5 kV accelerating voltage (Figure 2.21).

2.2.2 System Used

The function of the illuminating/imaging system is to produce and direct an electron beam on to the sample. It comprises an electron gun and several magnetic lenses as indicated in Figure 2.22. The major components of the electron gun are the filament, an apertured shield and an anode. Electrons are produced from the filament by the

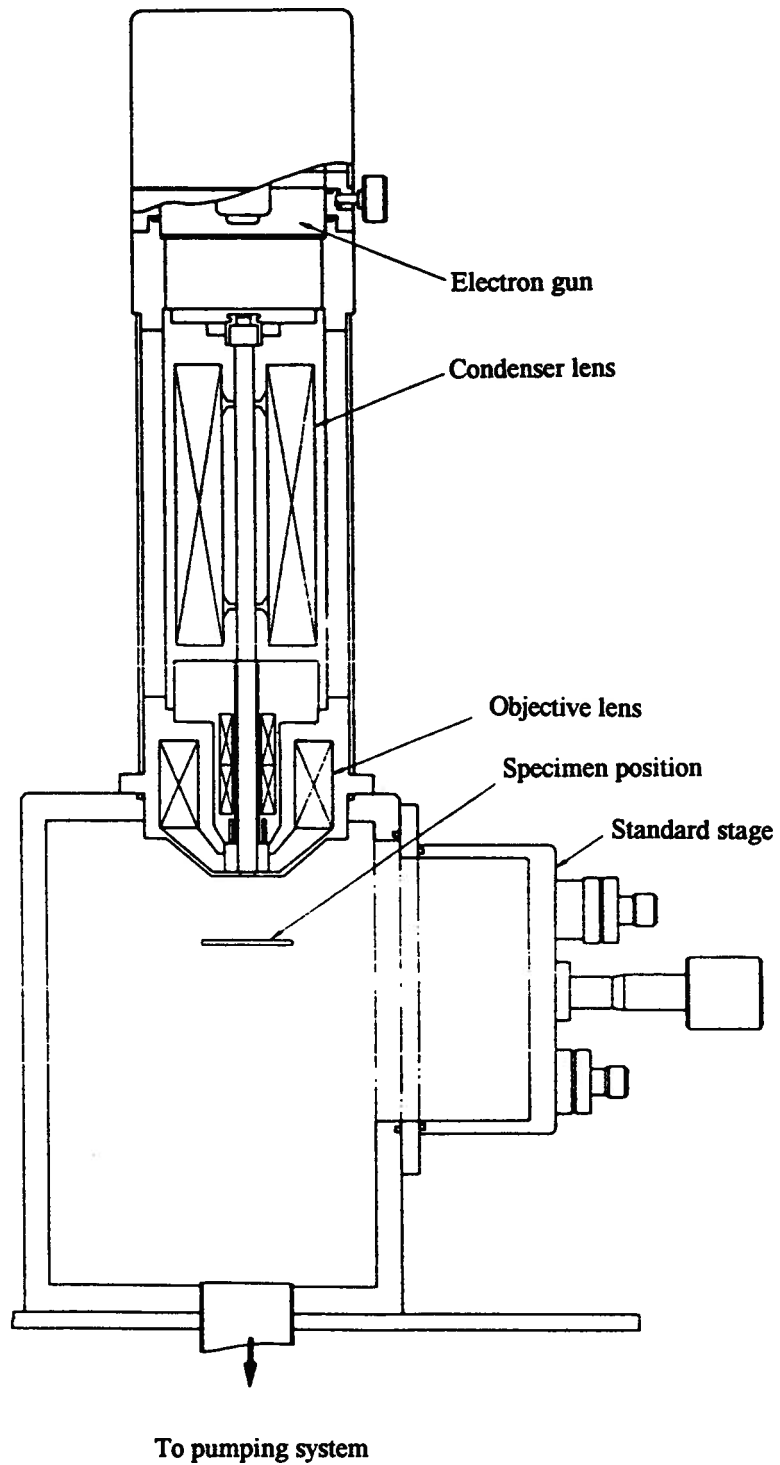


Figure 2.21 A schematic diagram of a scanning electron microscope (SEM).

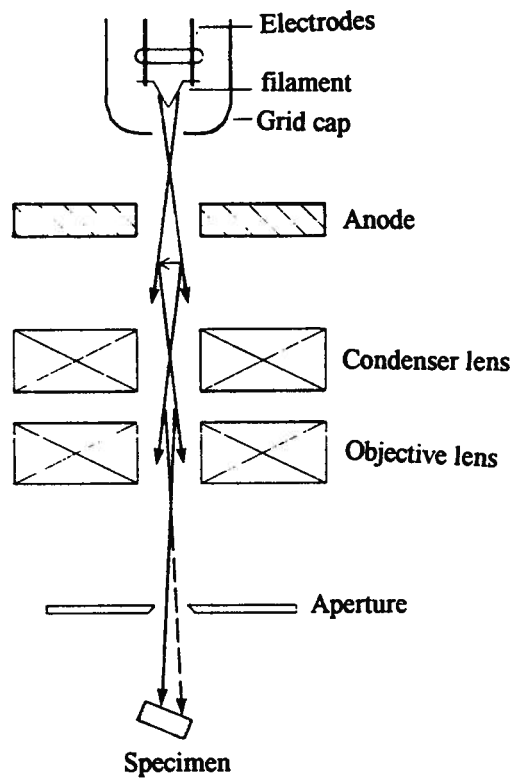


Figure 2.22 The illuminating / imaging system of a SEM unit.

thermionic effect, and an accelerating voltage is applied between the filament and anode. The apertured shield, or grid cap, is a slightly biased cylindrical cap which serves to collimate the electrons from the filament and direct them to the anode. The electron beam is then focused from a diameter of about 25000Å to 100Å by a series of magnetic lenses, and directed on to the sample. As a rule, the smaller the beam diameter, or the spot size, the higher the resolution.

The information system consists of the sample, which releases the electron signals resulting from interaction with the imaging beam, and the detectors, which recognize and analyze the signals. The sample is mounted on a conductive substrate and secured within the sample stage of the microscope. The stage serves as an electrical pathway to ground, and is also equipped with several controls for linear movement. The electron signals generated from the collision of the electron beam with the sample are detected by an imaging detector.

SEM images are displayed on the screen of a cathode-ray tube (CRT) and the scanning electron micrographs can be photographed for permanent record.

The SEM chamber is operated under vacuum ($\leq 10^{-4}$ torr) to avoid scattering between the electron beam and the residual gas. Also, this condition can help slow oxidation of the X-ray gun filament and limit contamination of the sample. The chamber is pumped by tubomolecular pumps backed by rotary pumps.

2.3 Weight Loss Measurements

Weight loss measurements [2.27] allow determination of the amount of corrosion occurring for a sample in a specific environment. In practice, the measurements are done by measuring the weight of the sample before corrosion (w_1), then exposing the sample to the corrosion environment, and then measuring the weight of the sample again after corrosion and cleaning of the sample surface (w_2). The corrosion rate can be calculated according to:

$$\text{Corrosion rate} = (K \times W) / (A \times T \times D) \quad (2.19)$$

where $W = w_1 - w_2 =$ the total weight loss (g)

$A =$ surface area of the sample (cm^2)

$T =$ time of exposure in the corrosion environment (hour)

$D =$ density of the sample (g/cm^3)

$K =$ a constant

($= 2.78 \times 10^6 \times D$ if corrosion rate is expressed in $\mu\text{g}/\text{m}^2\text{s}$)

In our work, the corrosion environment employed for the weight loss measurements is immersion in a 3.5% NaCl solution for 2 hours at room temperature. After this treatment, the sample is chemically cleaned by immersing in concentrated nitric acid for 15 minutes at room temperature to remove any corrosion products from the surface. The sample is then rinsed with distilled water, vacuum dried, and weighed. All weighings were done on an analytical balance to 0.0001g.

2.4 Atomic Absorption Spectrometry

In this work, atomic absorption spectrometry (AAS) [2.28] is applied to detect the dissolution of aluminum ions (Al^{3+}) from the sample during treatment in a corrosive environment. This method is used as a supplement to evaluate the corrosion protection performance of the zinc phosphate treated aluminum alloy surface. The 3.5% NaCl solution which is used for the corrosion test is analyzed by AAS to detect the presence of Al^{3+} . The absorbance is measured at wavelength of 309.21 nm by a Perkin Elmer 305A atomic absorption spectrometer using a N_2O /acetylene flame as the atomization source. Calibrations are done to correct the background by NaCl interference. The sensitivity of the method is about 0.01 ppm.

Chapter 3 Coating and Corrosion Studies on ZPO treated Aluminum Surfaces

3.1 Coating Studies on Zinc Phosphate Treated Aluminum Surfaces

3.1.1 Sample Preparations

The samples studied in this part of the work are designated by labels A to G (Table 3.1). A flow chart which summaries the whole sample preparation steps is shown in Figure 3.1. The 7075-T6 aluminum sheets, which contain about 6 % of zinc, 3 % of magnesium, 2 % of copper, 0.5 % of iron, 0.4 % of silicon, 0.2 % of titanium, 0.3 % of manganese and aluminum with the rest of the composition [3.1], were obtained from the Defence Research Establishment Pacific (DREP). They were cut into 1 cm x 1 cm panels for the experimental purpose. These panels were all polished to a mirror-like appearance (0.05 μ m finish) and then degreased with acetone and methanol. The coating processes were done by suspending these test panels in 10 wt.% zinc phosphate (ZPO) suspension at different pH conditions for 1 hour at room temperature. The acidity and basicity of the coating solution were adjusted by acetic acid (HOAc) and sodium hydroxide solution (NaOH) respectively. After coating, some panels were ultrasonically rinsed in distilled water for 1 min., while some of them were just normally rinsed in distilled water. All the panels were then rinsed with absolute ethanol and air-dried, followed by the XPS analyses.

3.1.2 XPS Measurements

XPS spectra were measured in a Leybold MAX 200 spectrometer at an operating pressure of 4.5×10^{-9} torr. The unmonochromatized MgK α radiation source (1253.6 eV)

Table 3.1 Sample descriptions.

<u>Code in text</u>	<u>Description</u>
A	7075-T6 aluminum panel polished to 0.05 μm finish, followed by degreasing with acetone and methanol.
B	Sample A treated in natural zinc phosphate (ZPO) solution (pH=6.6) without ultrasonic rinsing afterwards.
C	Sample A treated in natural zinc phosphate (ZPO) solution (pH=6.6) with ultrasonic rinsing afterwards.
D	Sample A treated in ZPO solution adjusted at pH=13.0 by NaOH with ultrasonic rinsing afterwards.
E	Sample A treated in ZPO solution adjusted at pH=10.5 by NaOH with ultrasonic rinsing afterwards.
F	Sample A treated in ZPO solution adjusted at pH=5.0 by HOAc with ultrasonic rinsing afterwards.
G	Sample A treated in ZPO solution adjusted at pH=3.5 by HOAc with ultrasonic rinsing afterwards.

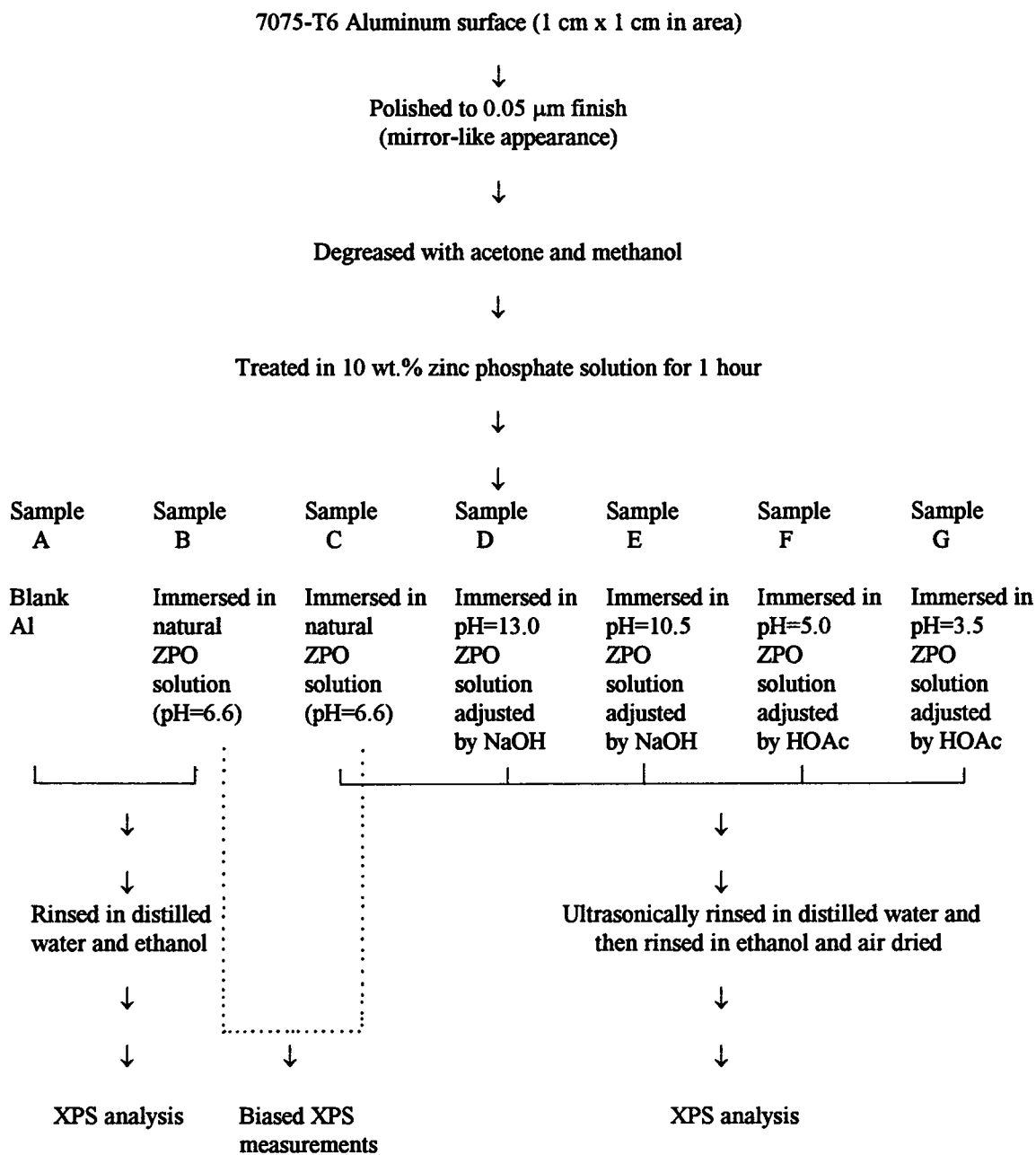


Figure 3.1 A flow chart summarizing the sample preparation procedure for the coating process.

was operated at 15 kV and 20 mA. Survey spectra for use in qualitative analysis were obtained with the pass energy of the hemispherical analyzer set at 192 eV; higher-resolution narrow scan spectra were measured for the Zn 2p_{3/2}, O 1s, C 1s, P 2p and Al 2p core levels at a 48 eV pass energy. For the latter, integrated peak areas determined after background subtraction were taken to measure relative elemental amounts after correction with the appropriate sensitivity factors provided by the manufacturer. Core level binding energies were referenced to the gold 4f_{7/2} binding energy at 84.0 eV. Narrow scan spectra were also measured for different values of the take-off angle (θ). A negative bias potential (-94 V) was applied to sample B and C during the biased experiments. The biased spectra obtained were shifted back by 94 eV for comparison with non-biased spectra.

3.1.3 Results and Discussion

(A) The Aluminum Control Panel (Sample A)

The XPS survey spectrum of sample A indicates the presence of oxygen, carbon, and aluminum on the surface (Figure 3.2), as identified from the O 1s, C 1s and Al 2p photoelectron peaks. The carbon signals arise from airborne contamination or residual acetone and methanol in the degreasing procedure. The oxygen signals come from the oxygen component of various compounds on the surfaces, e.g. air-borne contamination, residual organic compounds and metal oxide. High resolution XPS spectrum of Al 2p photoelectron peak (Figure 2.7, as discussed in section 2.1.3 (A) of Chapter 2) shows the presence of both aluminum oxide (AlO_x) at binding energy of 74.1 eV and metallic aluminum at binding energy of 71.5 eV. Quantitative analysis and angle dependent XPS are performed, and the results are shown in Table 3.2. It is found that the composition ratio of the oxide peak to the metallic peak of aluminum increases with decreasing the

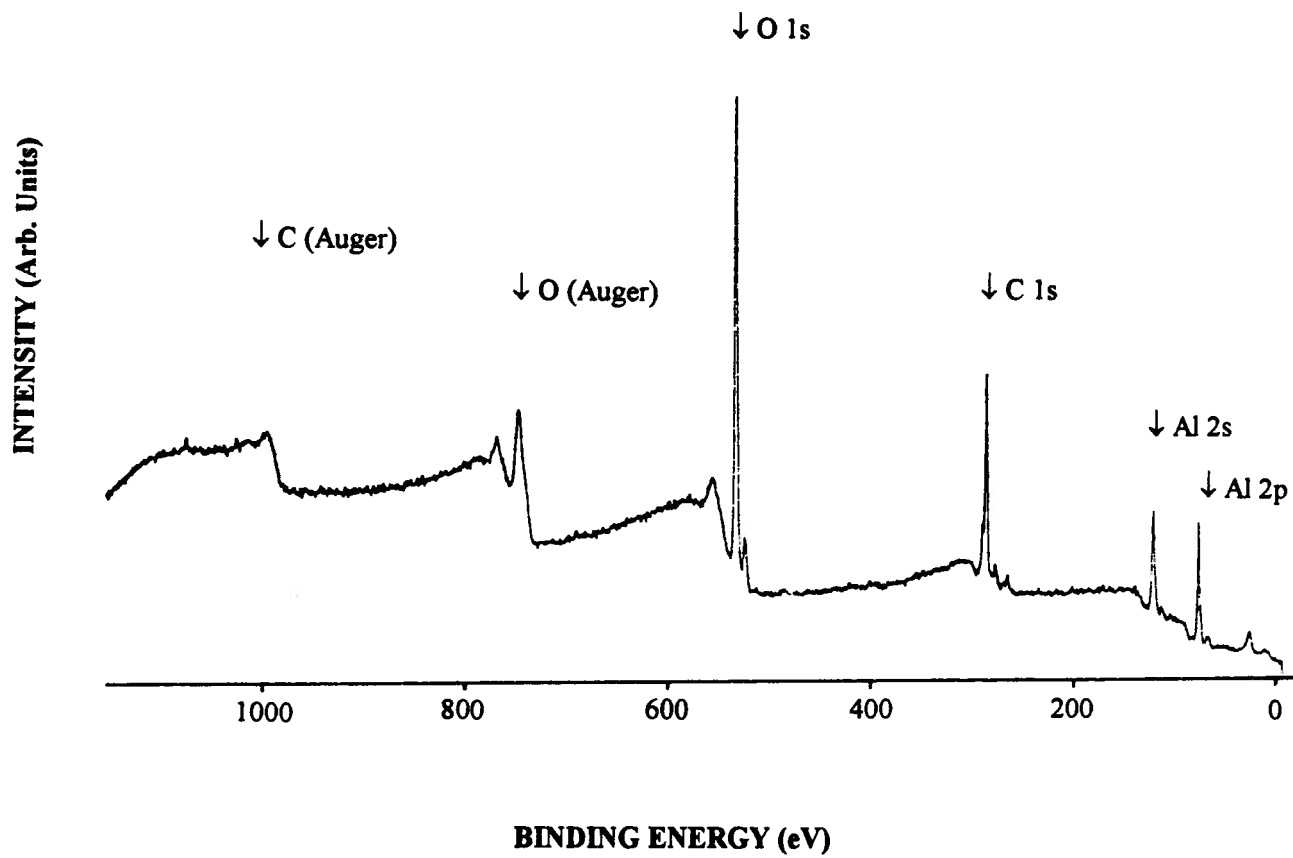


Figure 3.2 XPS survey spectrum for sample A, a blank Al surface.

Table 3.2 Elemental composition and atomic ratios for blank Al surface (sample A) with varying take-off angle, θ .

θ	[‡] Elemental composition (%)				Atomic ratio AlO _x /Al
	O	*Al	AlO _x	**Al _(m)	
30°	71.2	28.8	27.1	1.7	16.6
45°	70.5	29.5	27.6	1.9	14.9
60°	69.8	30.2	27.9	2.3	12.1
90°	70.2	29.8	26.6	3.2	8.3

*Al indicates the total Al content.

**Al_(m) indicates the metallic Al content.

[‡]Carbon was not taken into consideration since it is mainly from contamination.

take-off angle. This behaviour matches the conventional expectation that the oxide layers are on the top of the bulk metal [3.2]. Also, the thickness of the oxide layers are estimated at around 36 Å [3.3], using the inelastic mean free path values of 23 Å for AlO_x and 32 Å for metallic Al [3.4]. It is noteworthy that on this blank aluminum surface, no other alloy composition (e.g. zinc or magnesium) is detected.

(B) The Aluminum Panel Treated in Natural ZPO Solution at pH=6.6 (Samples B and C)

The coating processes for both sample B and sample C are similar, in which they are treated in natural zinc phosphate solution (with pH=6.6) for 1 hour at room temperature, except sample B without ultrasonic rinsing afterwards but sample C with ultrasonic rinsing (Figure 3.1). Qualitatively, the XPS survey spectra for the two samples look the same, both showing the presence of zinc in addition to oxygen, carbon and aluminum. The spectrum for sample C is shown in Figure 3.3. In both samples, however, no phosphorus is detected.

Biased and non-biased XPS measurements were performed on samples B and C. The high resolution spectra of Zn 2p_{3/2} photoelectron peaks for samples B and C at take-off angles of 90° and 30° obtained from non-biased XPS measurements are shown in Figure 3.4 (a) to (d). It is clear that two forms of zinc are present in sample B, with binding energies of 1026.7 eV and 1023.3 eV, but only the second one is well-established in sample C. With variation of the take-off angle, the intensity of the 1026.7 eV peak is enhanced at $\theta = 30^\circ$, showing that this higher binding energy component is located at the topmost region of the surface. Bias potential technique is applied to sample B and sample C. The resulting spectra, after shifting the measured spectra back by 94 eV, are shown in Figure 3.4 (e) and (f). It is found that the negative bias potential technique has no effect

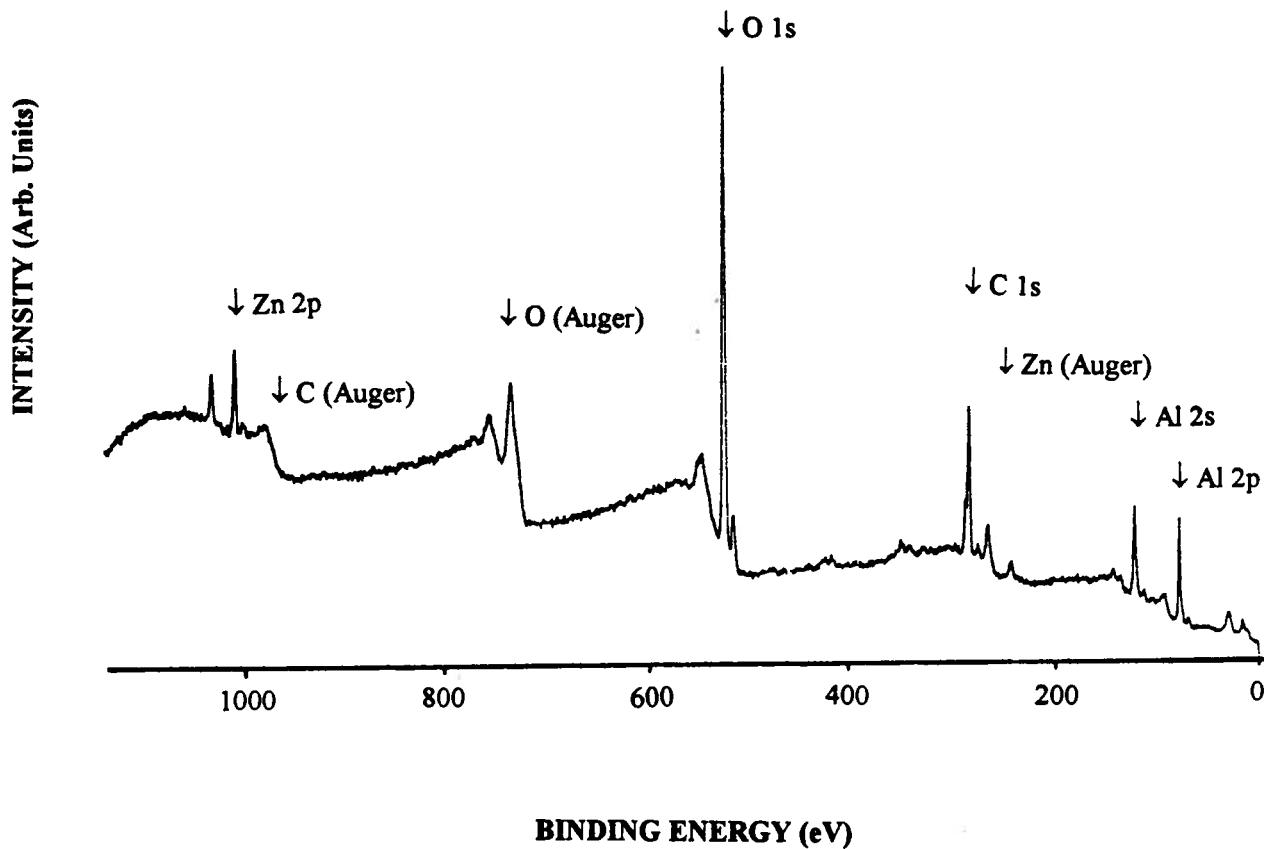


Figure 3.3 XPS survey spectrum for sample C, ZPO treated Al surface prepared at natural pH.

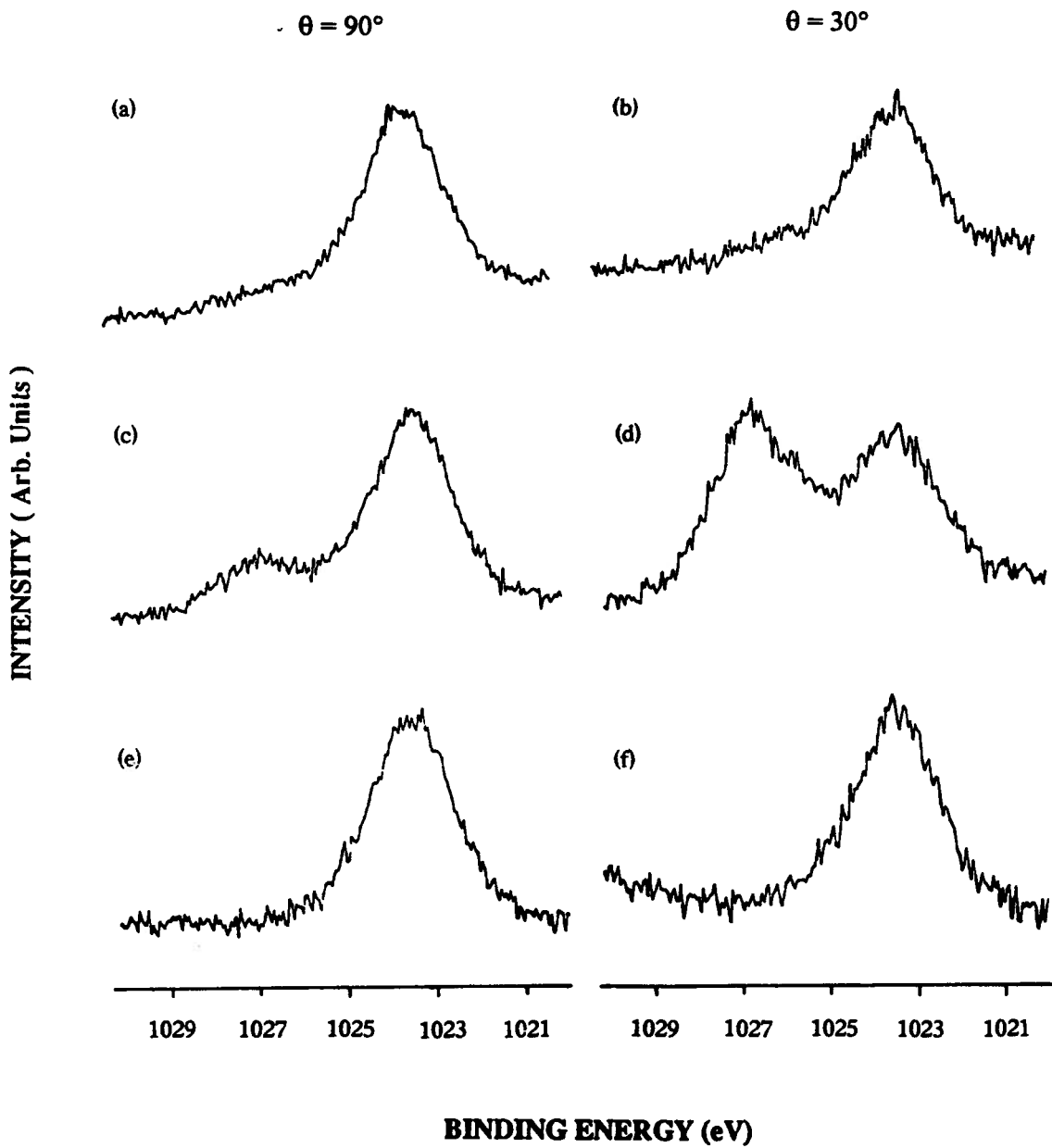


Figure 3.4 High resolution Zn 2p_{3/2} spectra for: (a) sample C, $\theta = 90^\circ$; (b) sample C, $\theta = 30^\circ$; (c) sample B, $\theta = 90^\circ$; (d) sample B, $\theta = 30^\circ$; (e) sample B, $\theta = 90^\circ$ after bias potential; (f) sample B, $\theta = 30^\circ$ after bias potential.

on the lower binding energy component, which still lies at 1023.3 eV after the measured spectra are shifted back. On the contrary, the higher binding energy component disappears in the spectra, suggesting that it is not in good electrical contact with the metal [3.5]. It is concluded that the 1026.7 eV component corresponding to zinc is weakly bonded or physically trapped at the surface; thereby it can be lost by ultrasonic rinsing, and it is not observed in sample C. The lower binding energy component (1023.3 eV), on the other hand, binds strongly at the surface. Therefore, it is not affected by the biased XPS measurements or the ultrasonic rinsing procedure. In conclusion, the ultrasonic rinsing in distilled water, which removes all the physically trapped species on the treated surfaces, is essential in the sample preparation procedure.

For the chemically absorbed zinc in the surface, the sum of its Auger parameter (α) and the excitation energy (1253.6 eV) equals 2010.0 eV, which is consistent with the component arising from an oxide ZnOx [3.6]. Quantitative and angle dependent XPS are done on sample C. The results are listed in Table 3.3. Comparing with the blank Al surface, there is a significant increase in the amount of zinc in sample C. The Zn/Al ratio essentially shows an angle independent behaviour, suggesting that ZnOx forms a mixture with the AlOx [3.7]. Figure 3.5(a) and (b) schematically indicates the morphologies proposed for these ZPO treated alloy surfaces.

The presence of zinc on the treated surface originates from the ZPO compound. ZPO is slightly soluble in water [3.8].



The zinc ions exist as a hydrated form, $\text{Zn}(\text{H}_2\text{O})_4^{2+}$, in solution and also hydrolyze in water, giving a slightly acidic coating solution [3.9].

Table 3.3 Elemental composition and atomic ratios for ZPO treated Al surface (sample C) with varying take-off angle, θ .

θ	[†] Elemental composition (%)			Atomic ratio
	O	Al	Zn	Zn/Al
30°	74.3	24.5	1.2	0.05
45°	72.3	26.0	1.7	0.06
60°	71.2	26.9	1.9	0.07
90°	71.9	26.2	1.9	0.07

[†]Carbon was not taken into consideration since it is mainly from contamination.

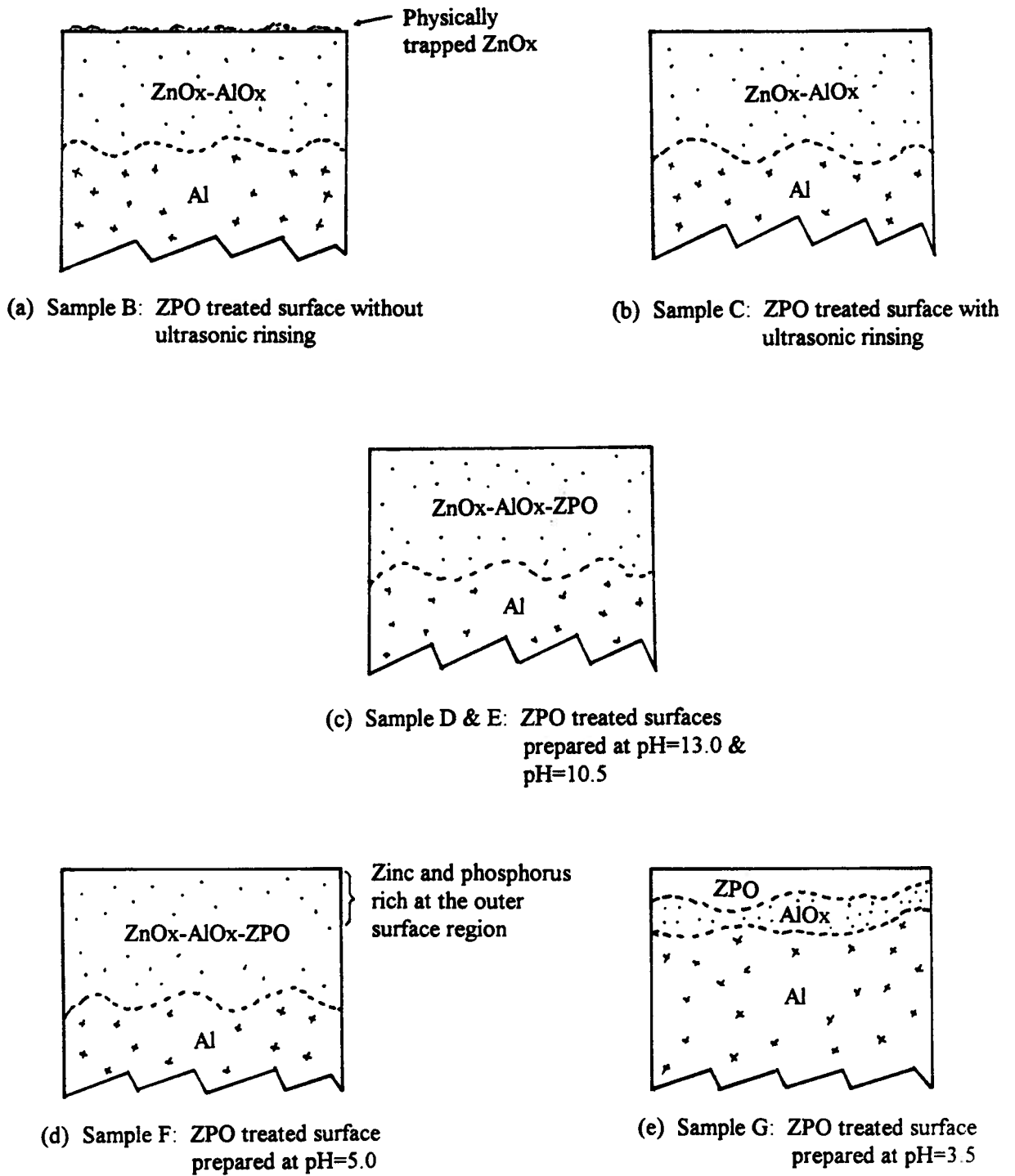
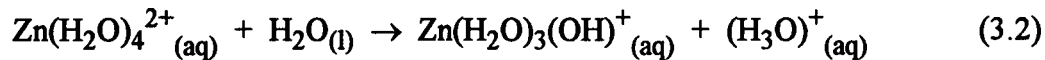


Figure 3.5 Proposed surface morphologies for (a) sample B, (b) sample C, (c) samples D & E, (d) sample F and (e) sample G.



The hydrated zinc ions are believed to interact with the alloy surface, and incorporate deeply into the aluminum oxide matrix, thereby forming a AlO_x-ZnO_x mixture. Phosphorus, though, may be adsorbed on the surface, but it is undetectable by XPS. This behaviour provides a reference point with which to compare the samples prepared in alkaline and acidic coating solutions.

(C) The Aluminum Panel Treated in ZPO Solution at Various pH Values (Samples D to G)

After the ZPO treatments, all the four samples (samples D, E, F and G) retain a mirror-like appearance. Based on the discussion in Section B, these treated samples are ultrasonically rinsed in distilled water to remove any physically trapped zinc component. XPS analyses are performed and their XPS spectra look similar, except that the intensity of the photoelectron peaks are different. The XPS survey spectrum of sample D is shown in Figure 3.6. It is observed that besides oxygen, carbon and aluminum, zinc and phosphorus are detected on these four samples. The high resolution XPS spectrum of Al 2p peak shows that it contains both oxide and metallic components, lying at binding energies of 74.1 eV and 71.5 eV.

The binding energies of zinc and phosphorus and the kinetic energies of zinc L₃M₄₅M₄₅ Auger lines measured on these surfaces are listed in Table 3.4. The table also gives the values obtained from the ZPO reference compound for comparison. The binding energies of Zn 2p_{3/2} photoelectron peaks lie between 1023.1 eV and 1023.7 eV, and the sums of the Auger parameters of Zn and the excitation energy are in the range of 2010.1

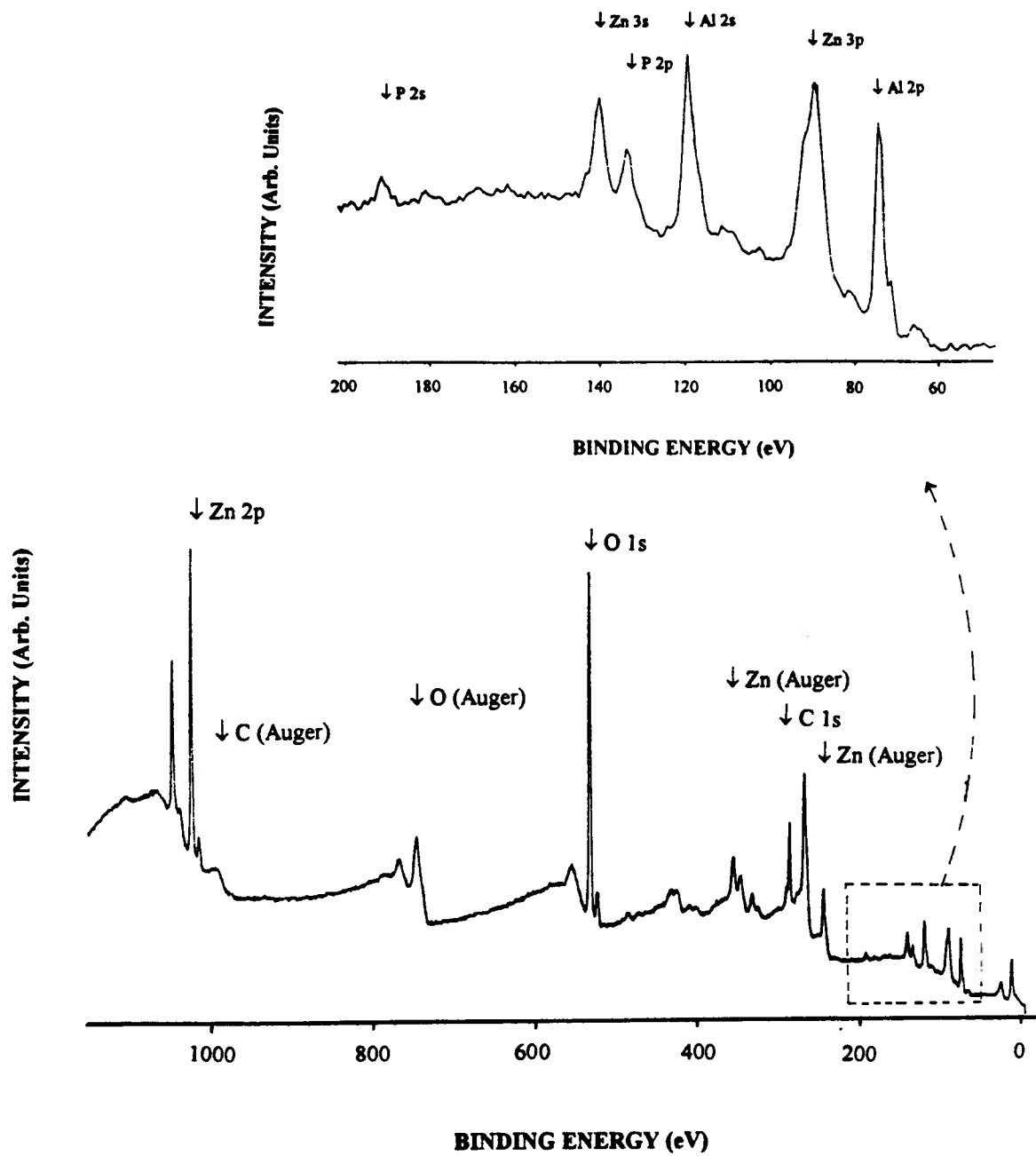


Figure 3.6 XPS survey spectrum for sample D, ZPO treated Al surface prepared at pH=13.0.

Table 3.4 A list of binding energies (in eV) of zinc, phosphorus on ZPO treated aluminum surfaces and the ZPO reference compound.

Sample	Zn 2p _{3/2} [†]	Zn Auger [†] L ₃ M ₄₅ M ₄₅	α+hν*	P 2p [†]	C 1s [†]
ZPO reference compound	1023.7	988.6	2010.3	133.7	285.0
C (at pH=6.6)	1023.3	987.1	2010.4	--	285.0
D (at pH=13.0)	1023.4	986.9	2010.3	133.5	285.0
E (at pH=10.5)	1023.5	987.0	2010.5	133.7	285.0
F (at pH=5.0)	1023.6	987.0	2010.6	133.7	285.0
G (at pH=3.5)	1023.1	987.0	2010.1	133.9	285.0

[†] The values of the binding energies of Zn 2p_{3/2}, P 2p and C 1s photoelectrons (in eV)
The values of the kinetic energy of the Zn Auger L₃M₄₅M₄₅ electrons (in eV)

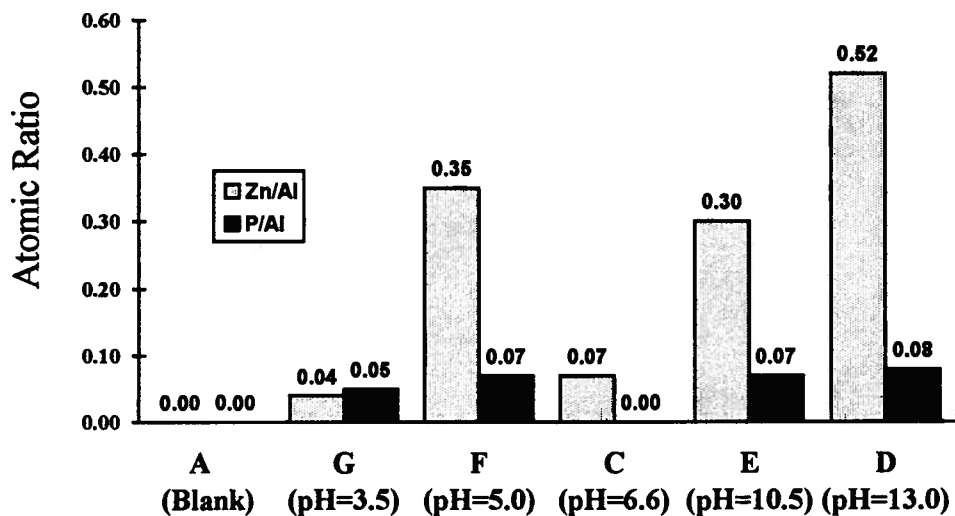
* The excitation source energy (hν) equal to 1253.6 eV

to 2010.6 eV, consistent with a ZnOx [3.6], although very similar values (1023.7 eV and 2010.3 eV respectively) were measured for the ZPO reference compound. Therefore, it was not possible to discriminate between these forms in relation to zinc (i.e. this metal is present in the +2 oxidation state). The measured P 2p photoelectron peaks lie between 133.5 eV and 133.9 eV, matching the value (133.7 eV) of the ZPO reference compound. Therefore, the chemical state of phosphorus on the treated surfaces is in the form of phosphate (i.e. in the +5 oxidation state).

Figure 3.7(a) shows the pH effect on the samples of the atomic ratios of zinc to aluminum and phosphorus to aluminum measured at $\theta = 90^\circ$. It is found that starting from pH=6.6 of the ZPO coating solution, the amounts of zinc and phosphorus on the alloy surface increase with the pH to 10.5 and 13.0. However, with decreasing pH from 6.6, the amount of coated zinc and phosphorus is increased at pH=5.0 and decreased at pH=3.5. Angle dependent XPS and quantitative analysis (Table 3.5) reveal the distributions of zinc and phosphorus on the surfaces. Values of Zn/P ratios can be used to follow the trends in composition, although it is not generally possible to relate to absolute compound composition. For example, the ratio measured for the ZPO reference compound is 0.88. Aside from any uncertainties in the atomic sensitivity factors, differences from the value of 1.5, predicted by the formula $\text{Zn}_3(\text{PO}_4)_2$, may be expected to arise from changes in surface composition (e.g. this ratio will vary markedly with involvement by HPO_4^- and $\text{H}_2\text{PO}_4^{2-}$ ions near the surface of the reference material).

The following subsections summarize the XPS observations for each coating solution and discuss in terms of the solution and interface chemistry that are likely to be relevant to the observations.

(a) Before corrosion



(b) After corrosion

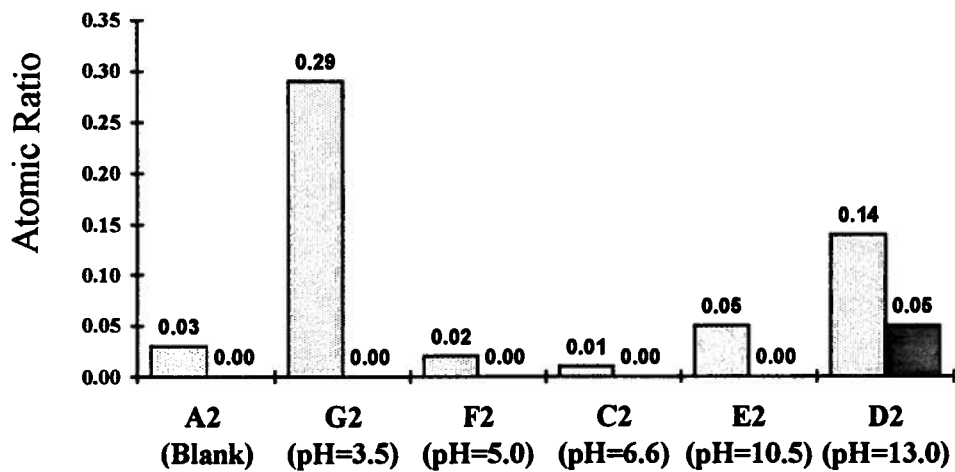


Figure 3.7 pH effect on the atomic ratios of elements on the ZPO treated Al surfaces (a) before and (b) after corrosion tests (values obtained at take-off angle equal 90°).

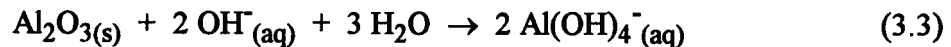
Table 3.5 Atomic ratios for samples C, D, E, F, G, and the ZPO reference compound with varying take-off angle, θ .

Sample	θ	Zn/Al	P/Al	Zn/P
ZPO reference compound	--	--	--	0.88
C (at pH=6.6)	30°	0.05	--	--
	45°	0.06	--	--
	60°	0.07	--	--
	90°	0.07	--	--
D (at pH=13.0)	30°	0.42	0.10	4.2
	45°	0.49	0.15	3.3
	60°	0.53	0.09	5.9
	90°	0.52	0.08	6.5
E (at pH=10.5)	30°	0.39	0.09	4.3
	45°	0.37	0.08	4.6
	60°	0.34	0.06	5.7
	90°	0.30	0.07	4.3
F (at pH=5.0)	30°	0.55	0.19	2.9
	45°	0.53	0.19	2.8
	60°	0.44	0.11	4.0
	90°	0.35	0.07	5.0
G (at pH=3.5)	30°	0.03	0.10	0.3
	45°	0.03	0.06	0.5
	60°	0.04	0.06	0.7
	90°	0.04	0.05	0.8

(1) **Strongly Alkaline Coating Solution (pH=13.0; Sample D)**

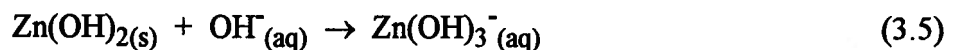
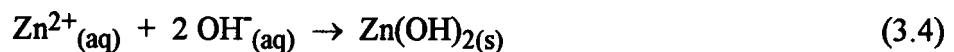
XPS studies (Table 3.5) show that large amounts of zinc and phosphorus are present on this treated alloy surface. The enhanced value of the Zn/P ratio (compared with ZPO) indicates that the surface is zinc rich, relative to phosphorus, possibly both ZnOx and ZPO being involved in the coating. Angle dependent XPS shows that the Zn/Al ratios vary slowly with the take-off angle, and the P/Al ratio is almost angle independent, implying that zinc and phosphorus are randomly distributed in the aluminum oxide mixture [3.7]. It is proposed that this coating is a mixed ZPO-AlO_x-ZnO_x material, as shown in Figure 3.5(c).

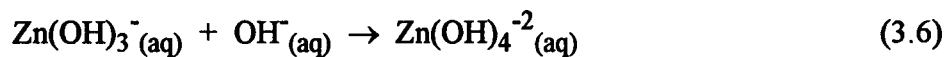
The formation of this layer is the result of both the etching and coating processes on the surface. The hydroxide ions present in this strong alkaline solution will react with the aluminum oxide on the alloy surface [3.9, 3.10].



The aluminum oxide layer is thus etched out, and therefore zinc, one of the constituents of the alloy composition, is exposed to the surface region.

On the other hand, the solubility of ZPO is enhanced because of the formation of zinc hydroxide and zinc hydroxide complexes [3.10].





These complexes, together with the increased amount of phosphate ions in the solution, are believed to interact with the freshly etched alloy and incorporate into the aluminum oxide matrix. It is expected that both the etching and coating processes occur concurrently, thus giving a ZPO-AlO_x-ZnO_x structure. Since the enhancement in solubility causes more zinc and phosphate ions in solution, larger amounts of zinc and phosphorus can be coated on the surface.

(2) Moderately Alkaline Coating Solution (pH=10.5; Sample E)

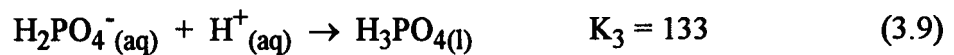
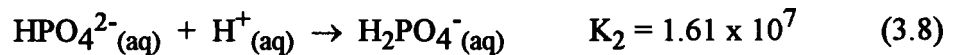
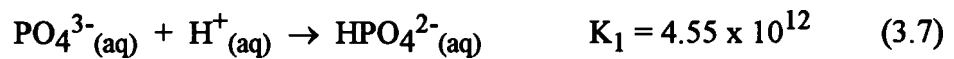
XPS studies indicate that the amounts of zinc and phosphorus on the alloy surface treated at this condition are less than that of sample D. XPS measured for different θ (Table 3.5) shows that the P/Al ratio is angle independent and the Zn/Al ratio slightly varies with the take-off angle, suggesting that the layer is a mixture of zinc, phosphorus and aluminum [3.7]. The Zn/P ratio indicates sample E is zinc rich, implying both ZnO_x and ZPO are present. It is believed that the surface morphology of this surface is similar to that of sample D, i.e. a mixture of ZPO-AlO_x-ZnO_x structure (Figure 3.5(c)). Also, the etching and coating processes are similar in both cases. However, with lower alkalinity for the coating solution at pH=10.5, a relatively milder etching process is expected. Thus, smaller amounts of zinc and phosphorus are found on the treated surface.

(3) Moderately Acidic Coating Solution (pH=5.0; sample F)

XPS studies (Figure 3.7(a)) indicate that more zinc and phosphorus are on sample F than on sample C. Angle-dependent XPS (Table 3.5) shows that both Zn/Al and P/Al ratios were almost unchanged at small take-off angles, but they decrease for the large

values of θ . This suggests that zinc and phosphorus are mixed in the AlOx matrix [3.7], but with distributions that are relatively richer at the outer surface region. The Zn/P ratio of sample F is larger than that of the ZPO reference compound, implying that the coating involves ZnOx and ZPO, and that etching and coating processes have occurred. A proposed surface morphology is shown in Figure 3.5(d).

At pH=5.0, the presence of H^+ ions in the ZPO coating solution enhances the solubility of ZPO because of the formation of hydrogen phosphate (HPO_4^{2-}), dihydrogen phosphate ($H_2PO_4^-$), and phosphoric acid (H_3PO_4) [3.12, 3.13].



The presence of ZnOx suggests that the etching process, possibly by phosphoric acid, has occurred on the surface, and thus exposed zinc from the substrate. Also, the enhanced solubility of ZPO in this medium ensures that the surface is exposed to Zn^{2+} and phosphate ions (e.g. $H_2PO_4^-$), which can be absorbed and incorporated into the AlOx matrix. This is consistent with the formation of a ZnOx-AlOx-ZPO coating on the alloy. Insofar as the zinc and phosphorus compositions are greater at the outer surface region, relative to the inner coating region, the precipitation of zinc appears to occur relatively faster than the zinc build up from the etching process.

(4) Strongly Acidic Coating Solution (pH=3.5; sample G)

XPS results (Figure 3.7(a)) indicate that the Zn/Al and P/Al ratios have the smallest values among the five treated alloy surfaces. However, it is found that the Zn/P ratio at $\theta=90^\circ$ (Table 3.5) is closest to that of the ZPO reference compound. The Zn/Al ratios appear constant with take-off angle; likewise the P/Al ratios are almost unchanged from 90° to 45° , although the ratio increases at $\theta = 30^\circ$, suggesting that more phosphorus is at the outermost surface region. Figure 3.5(e) shows the proposed surface morphology of sample G.

The low zinc to phosphorus ratio on this treated surface may result from the dissolution of the ZnOx-AlOx structure. At pH=3.5, phosphoric acid is a major component in the coating solution. This acid possibly etches the surface and exposes zinc from the substrate. However, relating to the observations, it is expected that the ZnOx-AlOx structure is unstable under strong acidic condition and is thereby removed from the surface. Moreover, the precipitate of ZPO is suppressed because of the strong acidic environment [3.14]. Consequently, the amounts of zinc and phosphorus on the treated surface are small.

3.2 Corrosion Studies on Zinc Phosphate Treated Aluminum Surfaces

3.2.1 Sample Preparations

The corrosion studies were divided into two parts. Part I was an initial test on samples A and C only; while Part II was a further study involving all the treated surfaces (samples A, C, D, E, F and G), which were prepared at different pH conditions.

Figures 3.8 and 3.9 summarize the sample preparation procedures for Parts I and II of these studies. In Part I (a), XPS and scanning electron microscopy (SEM) analyses were performed, as shown in Figure 3.8(a). Samples A and C, after the SEM examinations, were immersed in 3.5 % NaCl solution for 2 hours. After that, they were rinsed with distilled water and then air-dried. The resulting surfaces were designated as samples A1 and C1 respectively. Both XPS and SEM studies followed.

In Part I (b), weight loss and atomic absorption spectroscopy (AAS) analyses were performed, as shown in Figure 3.8(b), on blank 7075-T6 aluminum panels which were polished to a 220 grit finish (including 2 faces and 4 edges). After polishing, the panels were degreased with acetone and methanol. The coating process was done by suspending the test panels in 10 wt. % zinc phosphate solution (natural ZPO solution) for 1 hour at room temperature. After the ZPO treatment, the panels were ultrasonically rinsed in distilled water for 1 minute, followed by rinsing in absolute ethanol and then air-dried. Weight loss measurements were performed on these treated surfaces and blank surfaces respectively. After the tests, the 3.5% NaCl solution was analyzed by atomic absorption spectrometry to detect the presence of Al^{3+} ions.

(a) XPS and SEM examinations

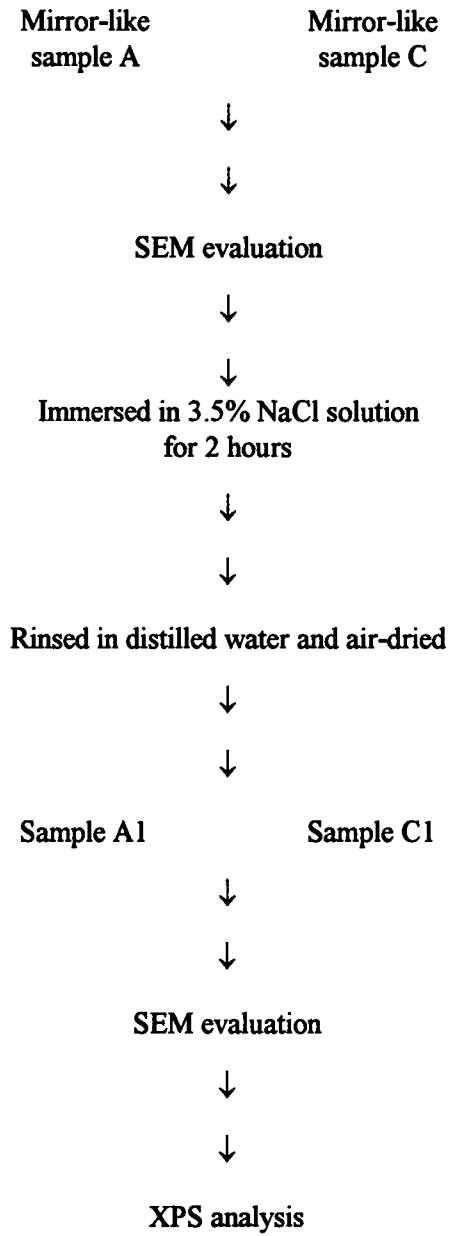


Figure 3.8 Sample preparation steps for Part I (initial studies) of corrosion studies.

(b) Weight loss and atomic absorption spectrometry analyses

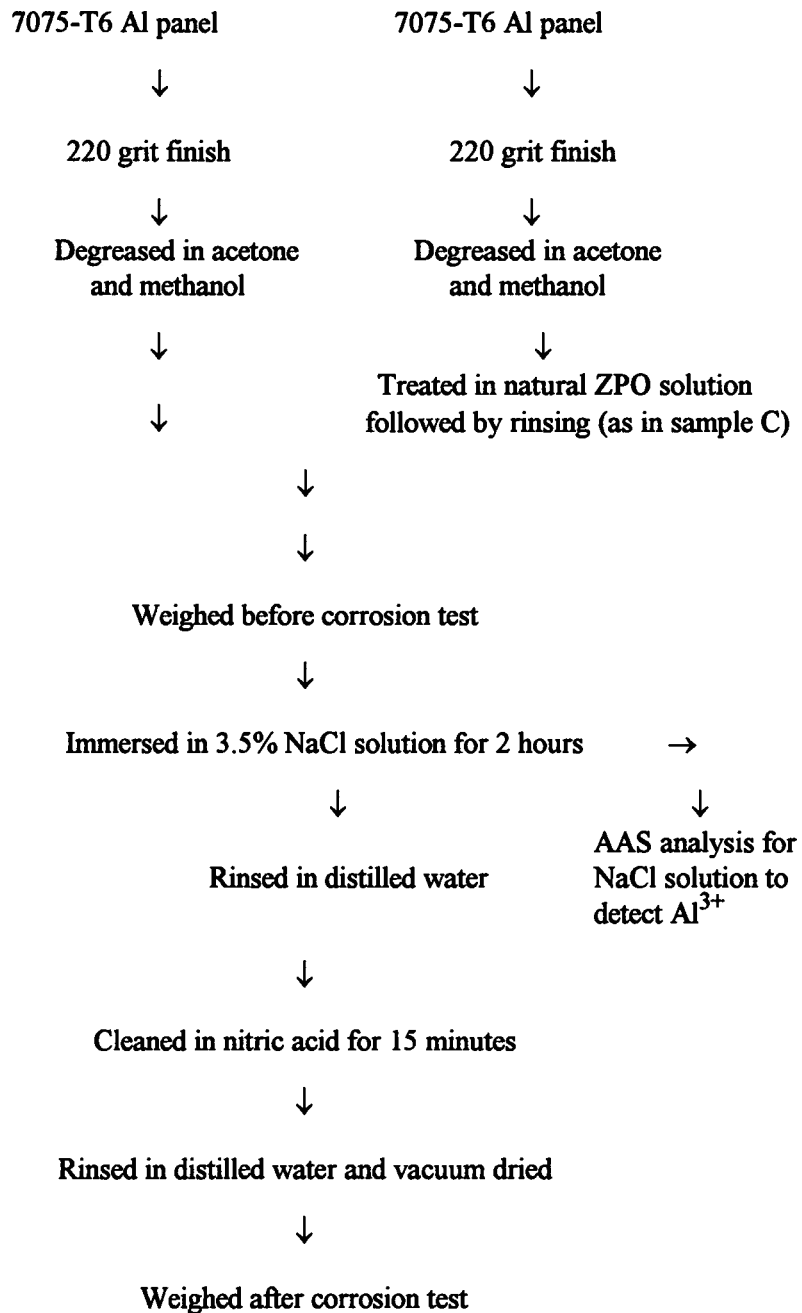


Figure 3.8 Sample preparation steps for Part I (initial studies) of corrosion studies.

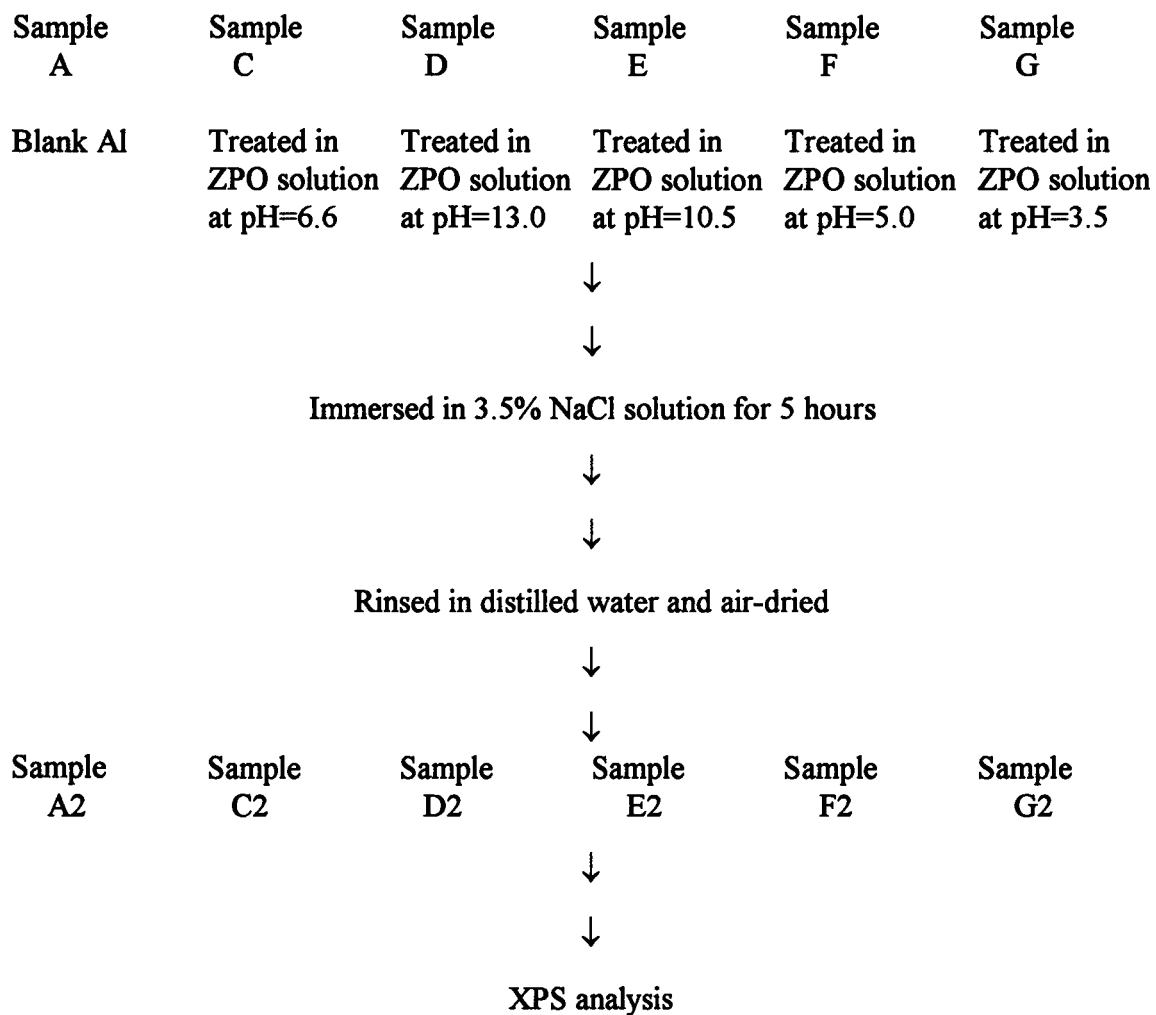


Figure 3.9 Sample preparation steps for Part II (further studies) of corrosion studies.

In Part II of the corrosion studies, as shown in Figure 3.9, samples A, C, D, E, F and G were immersed into 3.5% NaCl solution for 5 hours, followed by distilled water rinsing and air drying. The resulting surfaces were designated as A2, C2, D2, E2, F2 and G2 respectively. XPS analyses were performed on these surfaces.

3.2.2 Results and Discussion

(A)Part I: Initial Studies

Samples A and C after the corrosion test were analyzed by XPS. The atomic ratios obtained are listed in Table 3.6. It is found that zinc is present in sample A1, which is the surface of sample A after the corrosion test. High resolution XPS shows that this Zn $2p_{3/2}$ peak lies at binding energy of 1023.3 eV, implying that zinc exists as a form of zinc oxide (ZnOx). The presence of zinc in sample A1 suggests that immersion in the NaCl solution exposes zinc from the bulk aluminum alloy. Angle dependent XPS measurements (Table 3.6) show that the Zn/Al ratio is independent of the take-off angle, indicating that ZnOx is distributed evenly within the aluminum oxide layer [3.7]. Only the AlOx at binding energy of 74.1 eV is detected on sample A1. No metallic Al is found. This suggests the sample has a further oxidation of aluminum metal to AlOx in the salt solution.

The Zn/Al ratios, measured at take-off angles of 90° to 45° , are similar for samples C and C1, as shown in Table 3.6. This suggests that immersion in the corrosive NaCl solution has no significant effect on the amount of zinc on the surface, and the surface structure created from ZPO treatment does not significantly change under the corrosion test condition for 2 hours. At take-off angle equal to 30° , the Zn/Al ratio of sample C1 increases, probably resulting from the effect of the preferential removal of AlOx at the outermost surface region and thus effectively building up ZnOx on the surface.

Table 3.6 Zn/Al ratios for samples A, A1, C and C1 with varying take-off angle, θ .

θ	Sample A	Sample A1	Sample C	Sample C1
30°	0.00	0.01	0.05	0.09
45°	0.00	0.02	0.06	0.07
60°	0.00	0.02	0.07	0.06
90°	0.00	0.02	0.07	0.06

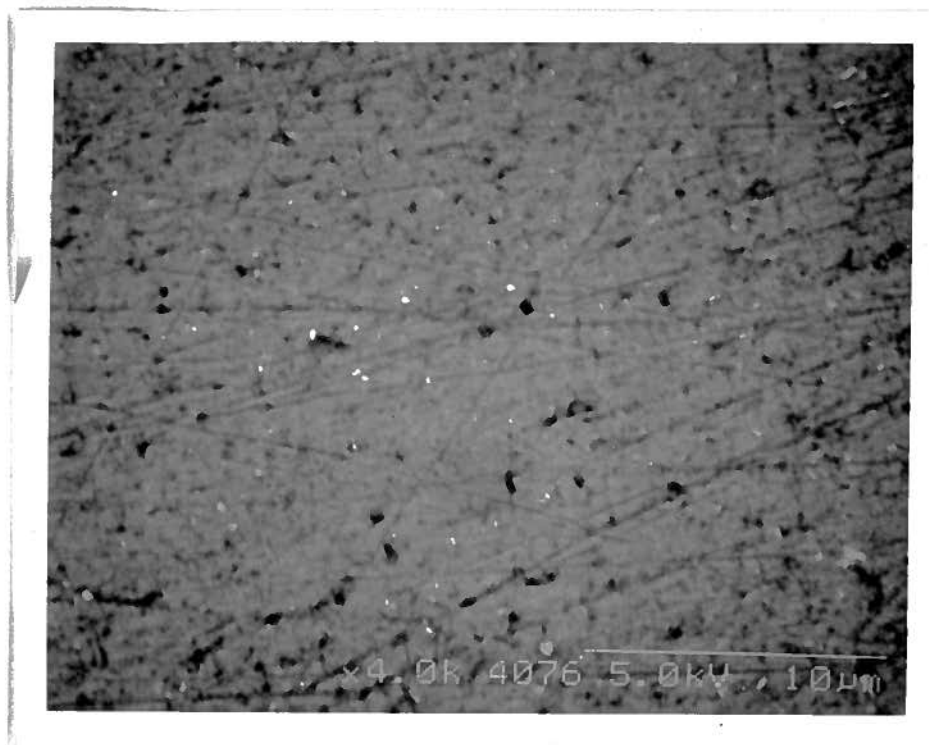
Consequently, there is relatively more zinc present at the outer surface region than at the inner region.

Figure 3.10 shows the SEM micrographs for samples A, A1, C and C1 respectively. Both samples A and C (Figure 3.10(a) and (c)), which are surfaces prior to exposure to 3.5% NaCl solution, have a similar flat appearance. However, after exposure to 3.5% NaCl solution, the appearance of a large corrosion area on sample A1 suggests that serious corrosion attack has occurred on this untreated aluminum surface. On the other hand, the corrosion areas on sample C1 are much smaller and the sample has most of the surface unchanged.

Weight loss measurements are used to determine the corrosion rates of the blank aluminum sample and the ZPO treated aluminum sample. After 2 hours exposure to 3.5% NaCl solution at room temperature, the corrosion rate for the blank sample is found to be $118 \mu\text{g}\cdot\text{m}^{-2}\cdot\text{s}^{-1}$. However, no detectable weight loss is observed for the treated surface. The results from atomic absorption spectrometry (AAS) are consistent with the weight loss measurements. About 0.2 ppm of Al is found in the 3.5% NaCl solution after the 2 hours corrosion test for the blank Al sample. By contrast, the Al concentration in the NaCl solution, in which the surface treated with ZPO is immersed, is below the detection limit of 0.01 ppm. These observations, together with the SEM and XPS analyses, show that a more serious corrosion attack occurs on the surface of sample A than on sample C.

The common point observed in previous studies of Cl^- attack on naturally formed aluminum-oxide covered aluminum is the dissolution of the metal [3.15-3.18], which is also observed in the present studies. Nguyen and Foley [3.15, 3.17, 3.18] proposed the following mechanism:

(a)



(b)

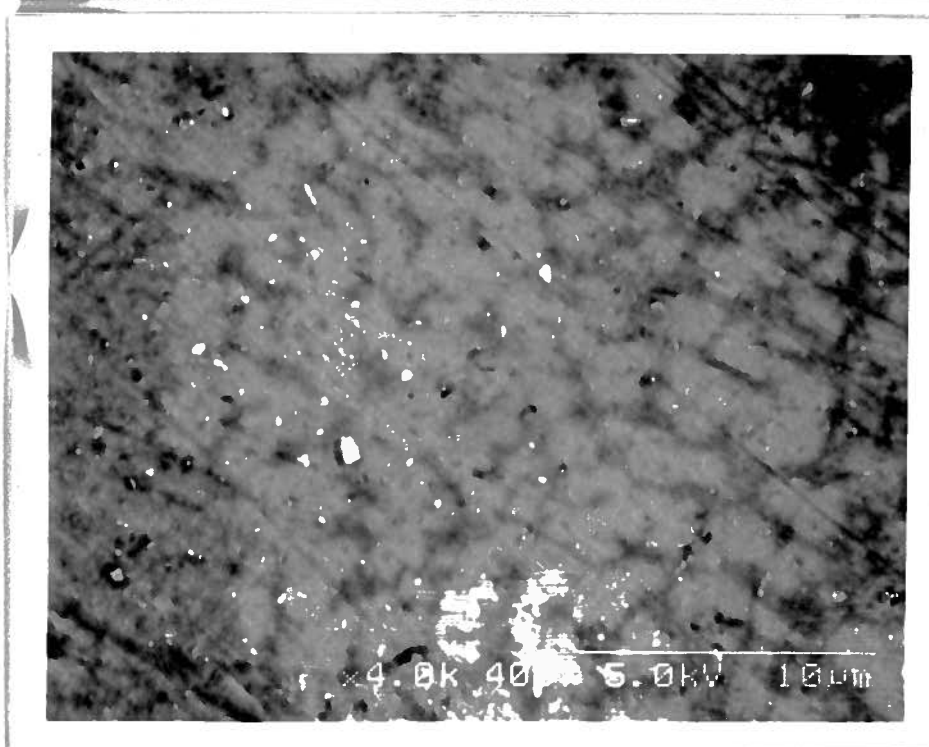


Figure 3.10 SEM micrographs of : (a) sample A, blank aluminum; (b) sample A1, sample A after corrosion; (c) sample C, ZPO treated aluminum; (d) sample C1, sample C after corrosion.

(c)

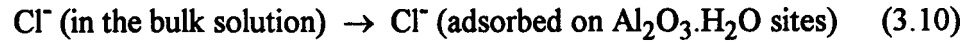


(d)

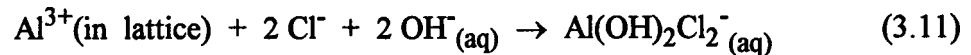


Figure 3.10 SEM micrographs of : (a) sample A, blank aluminum; (b) sample A1, sample A after corrosion; (c) sample C, ZPO treated aluminum; (d) sample C1, sample C after corrosion.

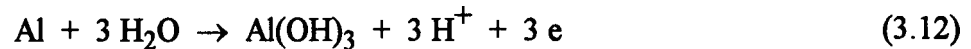
Step I: Adsorption on the oxide film



Step II: Chemical reaction



The product $\text{Al}(\text{OH})_2\text{Cl}_2^-$ is a soluble complex which is proposed to diffuse from reaction sites into solution. In the meantime, oxidation of the metallic Al occurs [3.17, 3.18]:



The results in the present work are consistent with this mechanism. Breakdown of the oxide film by Cl^- causes a rough and corroded surface appearance according to SEM investigation. The aluminum complex dissolving from the solid (Equation 3.11) contributes to the aluminum detected by AAS. Equation 3.11 is also consistent with the XPS observation that no Cl^- is detected on the 7075-T6 aluminum alloy surface after the corrosion test, which was first reported by Arnott *et al* [3.19]. Also, these authors failed to detect zinc on the blank surface but confirmed its presence after the corrosion test. The dissolution of aluminum from the ZPO treated surface is greatly suppressed, indicating that the zinc may strengthen the surface structure and thereby slow down the aluminum dissolution.

(B) Part II: Further Studies

The corrosion tests performed in this part of the study are extended from 2 hours to 5 hours. Results from XPS are summarized in Table 3.7. It is found that phosphorus is detected from sample D2, but not at all from the other surfaces. On the other hand, zinc, in the form of ZnO_x, is found on all the six samples, where some surfaces have an increase in the amount of zinc compared with the surfaces before corrosion, but some have a decrease. After the 5 hour corrosion attack, the metallic component of Al 2p photoelectron peak is detected on samples D2, E2, F2 and G2.

Figure 3.7(b) (on p.70) summarizes the quantitative results of the corrosion tests. As in the case of sample A1, the presence of zinc on sample A2 confirms that the Cl⁻ attack causes the dissolution of aluminum, thereby exposing zinc from the metal substrate to the surface region.

The extended corrosion test on sample C indicates that the amount of zinc decreases from sample C1 to sample C2, implying that the zinc originally coated on the surface dissolves into the solution during the corrosion process. Similar phenomena are also found on samples D to G. In addition, their amounts of phosphorus decrease to an undetectable level, except that Sample D2 has some residual amount of phosphorus. These phenomena imply that in such a corrosive condition, the ZnO_x-AlO_x-ZPO structure on the surface is damaged by the Cl⁻ attack, causing zinc and phosphorus to be removed from the surface. However, among the treatment conditions studied in this work, the one prepared in ZPO solution at pH=13.0 has the largest amounts of zinc and phosphorus on the surface, and likely has the strongest structure to defend against the corrosion attack.

Table 3.7 Qualitative observations from XPS for samples after immersion in NaCl solution.

Sample	Zinc*	Phosphorus*	Aluminum [†]
A2	Detected Amount increased	Not detected	Metallic Al not detected
C2	Detected Amount decreased	Not detected	Metallic Al not detected
D2	Detected Amount decreased	Detected Amount decreased	Metallic Al detected
E2	Detected Amount decreased	Not detected Amount decreased	Metallic Al detected
F2	Detected Amount decreased	Not detected Amount decreased	Metallic Al detected
G2	Detected Amount increased	Not detected Amount decreased	Metallic Al detected

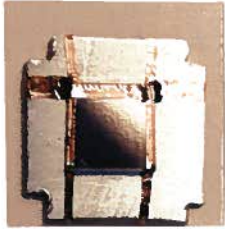
* The decrease or increase in the amount of zinc or phosphorus is compared with the same surface before immersion in NaCl solution.

[†] AlO_x always detected.

The detection of metallic Al on samples D2, E2 and F2 indicates the ZnO_x-AlO_x-ZPO layer on Al surface acts as a physical barrier [3.20], which is sacrificed in the corrosion attack, in the corrosion attack, thus slowing down the dissolution and oxidation of aluminum. Figure 3.11 shows the contrast between the blank Al surface and the ZPO treated surface prepared at pH=13.0. Figures 3.11(a) and (c) are the surfaces of samples A and C respectively. Before the corrosion test, they both have a shiny and silver-like appearance. Figure 3.11(b) and (d) shows the two surfaces after corrosion test. The surface of sample A2 turns brown and rough, while the surface of sample D2 only changes to a slightly yellow color with retention of its shiny appearance. The protected surface is clearly less corroded than the blank aluminum.

The significant increase of zinc content on sample G after corrosion presumably relates to its coating structure. The detection of metallic Al on sample G2 suggests that the coating on sample G is so ineffective, and the dissolution is so rapid that the oxide film attains only limited thickness. It is believed that the zinc from the treatment process has been removed and that the zinc detected on sample G2 comes from the alloy substrate. Possibly, the Cl⁻ ions induce the diffusion of zinc from the bulk to the surface region.

(a)



(b)



(c)



(d)

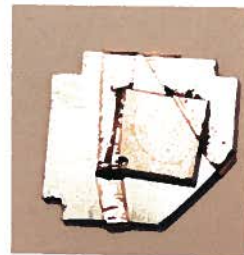


Figure 3.11 Photographs taken from surfaces after the 5 hours corrosion tests, (a) sample A, blank Al; (b) sample A2, sample A after corrosion; (c) sample D, ZPO treated surface prepared at pH=13.0; (d) sample D2, sample D after corrosion.

Chapter 4 Concluding Remarks and Future Work

4.1 Concluding Remarks

XPS studies on 7075-T6 aluminum surfaces treated in ZPO solution provide valuable information about the nature and the chemical properties of the coating [4.1]. Through these studies, it is concluded that zinc phosphate can provide an effective coating on aluminum alloy, although the results depend strongly on the coating pH. Also, biased XPS analysis reveals that ultrasonic rinsing on the surface after the ZPO treatment is needed to remove any physically adsorbed coating compounds from the surface, so as to ensure that a well-established coating is obtained.

The reactions occurring during the ZPO treatment are complex, because different processes, e.g. coating, etching, oxidation and bulk diffusion, occur concurrently but in different proportions under the various pH environments. The coatings formed in ZPO solution at pH=5.0, 10.5 and 13.0 have a mixed ZnO_x - AlO_x -ZPO structure, even though their atomic compositions and distributions are different. These variations are related to the different rates of etching and precipitation processes occurring at the alloy surfaces. The coating formed in natural ZPO solution (pH=6.6) is a ZnO_x - AlO_x mixed material, while the coating formed in ZPO solution at pH=3.5 exists as a thin ZPO-like compound. Among these pH conditions, the largest amounts of zinc and phosphorus were detected (for $\theta = 90^\circ$) on the surface treated at pH=13.0.

Corrosion studies show that the treated surfaces provide better corrosion control than the untreated one. The surface prepared at ZPO natural pH provides corrosion protection in 3.5 % NaCl solution for 2 hours. However, this surface is not strong enough

to defend for the extended 5-hour corrosion test. Among the treated surfaces under investigation, the one prepared at pH=13.0 is likely to give the best corrosion protection in the experimental corrosive environment. The studies show that zinc and phosphorus on the coating will dissolve and lose out from the surface under the Cl^- ions attack. Thus, the coating acts as a physical barrier sacrificing itself to slow down the oxidation and dissolution of aluminum under the corrosion attack. In terms of the amounts of zinc and phosphorus in the coatings from different pHs, it is likely that the greater the amounts of zinc and phosphorus on the coatings, the better is the corrosion control.

4.2 Future Work

Future research is suggested within the following approaches:

(1) Testing of other phosphate compounds

Phosphate compounds with other cation components, e.g. calcium phosphate, should be studied in order to determine the most effective compounds for coating and corrosion control on aluminum alloy materials. Also, these studies may be able to help investigate the effects of both the cation and anion components of the compounds on the coating process, and thus give a better understanding about the mechanism.

(2) Testing of organosilanes and phosphates mixtures

Organosilanes are used as additives in paint primers to improve the adhesion of paint on metal surface. Previous studies from our laboratory [4.2, 4.3] on the coating of organosilanes on aluminum indicate the presence of direct Si-O-Al bonding on the coated surface. It is suggested that the study of mixtures of silanes and phosphate compounds,

which is more close to the "real life" situation, should give a better understanding on their combination effect for both coating and corrosion protection.

References

- [1.1] D.Altenpohl, "Aluminum Viewed from Within" (Aluminum-Verlag, Düsseldorf, 1982) Chapter 1.
- [1.2] R.C.Weast, Ed., "Handbook of Chemistry and Physics" (CRC Press Inc., Cleveland, 1977) p.B-85.
- [1.3] B.C.Craig, Ed., "Handbook of Corrosion Data" (ASM International, Metals Park, 1989) p.16.
- [1.4] F.King, "Aluminum and its alloys" (Ellis Horwood Ltd., Chichester, 1987) Chapter 5.
- [1.5] S.Wernick, R.Pinner, P.G.Sheasby "The Surface Treatment and Finishing of Aluminum and its Alloys. Vol. I" (Finishing Publications Ltd., Teddington, 1987) Chapter 1.
- [1.6] P.A.Schweitzer, Ed., "Corrosion and Corrosion Protection Handbook" (Marcel Dekker Inc., New York, 1989) Chapter 1.
- [1.7] T.H.Nguyen and R.T.Foley, J. Electrochem. Soc. 127(1980)2563.
- [1.8] Ref. [1.1] p.185.
- [1.9] Ref. [1.5] Chapter 5.
- [1.10] I.Suzuki, "Corrosion-Resistant Coatings Technology" (Marcel Dekker Inc., New York, 1989) Chapter 5.
- [1.11] K.Hatanaka, M.Fukui, Y,Mukai, K.Toyose, Kobelco Tech. Rev. 6(1989)28.
- [1.12] T.Foster, G.N. Blenkinsop, P.Blattler and M.Szandorowski, J. Coat. Tech. 63(1991)91.
- [1.13] F.de.L.Fragata and J.E.Dopico, Surf. Coat. Internat. 74(1991)92.
- [1.14] T.Foster, G.N.Blenkinsop, P.Blattler and M.Szandorowski, J. Coat. Tech. 63(1991)101.
- [1.15] G.Adrian and A.Bittner, J. Coat. Tech. 58(1986)59.
- [1.16] W.J.Van Ooij and A.Sabata, Surf. Coat. Tech. 39/40(1989)667.
- [1.17] G.N.Bhar, N.C.Debnath and S.Roy, Surf. Coat. Tech. 35(1988)171.

- [1.18] N.Satoh and T.Minami, Surf. Coat. Tech. 34(1988)331.
- [1.19] A.Turuno, K.Toyose, H.Fujimoto, Kobelco Tech. Rev. 11(1991)14.
- [1.20] W.Rausch, "The Phosphating of Metals" (Finishing Publications Ltd., Teddington, 1990) Chapter 3.
- [1.21] D.B.Freeman, "Phosphating and metal pre-treatment" (Industrial Press Inc., New York, 1986) Chapter 2.
- [1.22] F.J.Spaeth, Mod. Paint. Coat. 74(1984)49.
- [1.23] D.J.O'Conuor, B.A.Sexton and R.St.C.Smart, "Surface Analysis Methods in Materials Science" (Springer-Verlag, Berlin, 1992) Chapter 1.
- [1.24] D.Briggs and M.P.Seah, Ed., "Practical Surface Analysis" (John Wiley and Sons Ltd., West Sussex, 1990).
- [1.25] Ref. [1.23] Chapter 5.
- [1.26] A.W.Czanderna and D.M.Hercules, Ed., "Ion Spectroscopies for Surface Analysis" (Plenum Press, New York, 1991) Chapter 6.
- [1.27] R.B.Ross, Ed., "Metallic Materials Specification Handbook" (Chapman & Hall, London, 1992).
- [1.28] P.E.Francis and T.S.Lee, Ed., "The Use of Synthetic Environments for Corrosion Testing, ASTM STP 970" (American Society for Testing and Materials, Philadelphia, 1988) p.217.
- [2.1] J.D.Andrade, "Surface and Interfacial Aspects of Biomedical Polymers. Vol. 1" (Plenum Press, New York, 1985) Chapter 5.
- [2.2] H.Hertz, Annal. Phys. 31(1887)982.
- [2.3] A.Einstein, Annal. Phys. 17(1905)132.
- [2.4] C.R.Brundle and M.W.Roberts, Proc. R. Soc. A331(1972)383.
- [2.5] B.L.Gabriel, "SEM: A User's Manual for Materials Science" (American Society for Metals, Metals Park, 1985) p.55.
- [2.6] Ref. [2.1] p.114.
- [2.7] Ref. [1.24] p.52.
- [2.8] S.Tanuma, C.J.Powell and D.R.Penn, Surf. Interface Anal. 11(1988)577.

- [2.9] S.Tanuma, C.J.Powell and D.R.Penn, Surf. Interface Anal. 17(1991)911.
- [2.10] S.Tanuma, C.J.Powell and D.R.Penn, Surf. Interface Anal. 17(1991)927.
- [2.11] D.R.Penn, J. Elect. Spect. Rel. Pheno. 9(1976)29.
- [2.12] M.P.Seah and W.A.Dench, Surf. Interface Anal. 1(1979)2.
- [2.13] C.D.Wagner, W.M.Riggs, L.E.Davis, J.F.Moulder and G.E.Muilenberg, Ed., "Handbook of X-ray Photoelectron Spectroscopy" (Perkin-Elmer Co., Eden Prairie, 1979) p.83.
- [2.14] D.Briggs, Ed., "Handbook of X-ray and Ultraviolet Photoelectron Spectroscopy" (Heyden & Son Ltd., London, 1977).
- [2.15] Ref. [2.1] p.123.
- [2.16] Ref. [2.13] p.84.
- [2.17] C.D.Wagner, Faraday Discuss. Chem. Soc. 60(1975)306.
- [2.18] Ref.[2.13] p.21.
- [2.19] D.Briggs and M.P.Seah, "Practical Surface Analysis" (John Wiley and Sons, Chichester, 1983) p.134.
- [2.20] Y.L.Leung, M.Y.Zhou, P.C.Wong, K.A.R.Mitchell and T.Foster, Appl. Surf. Sci. 59(1992)23.
- [2.21] A.J.Pertsin and Yu.M.Pashunin, Appl. Surf. Sci. 44(1990)171.
- [2.22] Max 200 User Manual (Leybold, Köln, Germany).
- [2.23] Ref. [1.24] Chapter 2.
- [2.24] J.M.Walls, Ed., "Methods of Surface Analysis" (Cambridge University Press, Cambridge, 1989) Chapter 3.
- [2.25] F.A.White and G.M.Wood, "Mass Spectrometry Applications in Science and Engineering" (Wiley-Interscience, New York, 1986) p.138-142.
- [2.26] Ref. [1.23] p.79-95.
- [2.27] 1985 Annual Book of ASTM Standards, Section 3, Metals Test Methods and Analytical Procedures, p.88-93 and p.176-185.
- [2.28] D.A.Skoog, "Principles of Instrumental Analysis" (CBS College Publishing, Philadelphia, 1985) p.250-291.

- [3.1] D.A.Jones, "Principles and Prevention of Corrosion" (Macmillan Publishing Co., New York, 1992).
- [3.2] C.S.Fadley, R.J.Baird, W.Siekhaus, T.Novakov and S.Å.L.Bergström, *J. Electro. Spect.* 4(1974)93.
- [3.3] J.Massies and J.P.Contour, *J. Appl. Phys.* 58(1985)806.
- [3.4] Ref. [2.12]
- [3.5] Y.L.Leung, M.Y.Zhou, P.C.Wong, K.A.R.Mitchell and T.Foster, *Appl. Surf. Sci.* 59(1992)23.
- [3.6] Ref. [2.14] Chapter 7.
- [3.7] B.D.Ratner, T.A.Horbett, D.Shuttleworth and H.R.Thomas, *J. Colloid Interf. Sci.* 83(1981)630.
- [3.8] W.F.Linke, "Solubility: Inorganic and Metal-organic Compounds, Vol. II" (American Chemistry Society, 4th ed., 1965) p.1680.
- [3.9] F.A.Cotton and G.Wilkinson, "Advanced Inorganic Chemistry" (John Wiley & Sons Inc., New York, 1972) Chapter 9.
- [3.10] G.F.Liptrot, "Modern Inorganic Chemistry" (Bell & Hyman Ltd., London, 1983) Chapter 17.
- [3.11] Ref. [3.10] Chapter 25.
- [3.12] D.E.C.Corbridge, "Studies in Inorganic Chemistry 10: Phosphorus" (Elsevier Science Publishers B.V., Amsterdam, 1990) Chapter 3.
- [3.13] Ref. [1.2].
- [3.14] F.J.Spaeth, *Mod. Paint & Coat.* 74(1984)49.
- [3.15] T.H.Nguyen and R.T.Foley, *J. Electrochem. Soc.* 127(1980)2563.
- [3.16] Z.A.Foroulis and M.J.Thubrikar, *J. Electrochem. Soc.* 122(1975)1296.
- [3.17] T.H.Nguyen and R.T.Foley, *J. Electrochem. Soc.* 126(1979)1855.
- [3.18] R.T.Foley and T.H.Nguyen, *J. Electrochem. Soc.* 129(1982)464.
- [3.19] D.R.Arnott, N.E.Ryan, B.R.W.Hinton, B.A.Sexton and A.E.Hughes, *Appl. Surf. Sci.* 22/23 (1985)236.

- [3.20] W.M.Morgans, "Outlines of Paint Technology" (Halsted Press, New York, 1990) Chapter 4.
- [4.1] W.F.Heung, Y.P.Yang, P.C.Wong, K.A.R.Mitchell and T.Foster, J. Mat. Sci. (accepted and in process).
- [4.2] Ref. [3.5].
- [4.3] Y.L.Leung, Y.P.Yang, P.C.Wong, K.A.R.Mitchell and T.Foster, J. Mat. Sci. Lett. 12(1993)844.